A Dissertation on

"MODELLING, SIMULATION AND TESTING OF A FEW POLARIZER COMPONENTS DEVELOPED AT INMAS, DRDO"

Submitted in the partial fulfillment of the requirements of the degree of

MASTER OF TECHNOLOGY

In

NUCLEAR SCIENCE & ENGINEERING

By

ANTO AUGUSTY

2K14/NSE/07

Under the Guidance of

Dr. Nitin K. Puri	**Mrs. Priyanka Sharma**
Assistant Professor	**Scientist 'C'**
DTU, New Delhi	**INMAS, DRDO**

DEPARTMENT OF APPLIED PHYSICS

DELHI TECHNOLOGICAL UNIVERSITY

NEW DELHI-110042

2016

INSTITUTE OF NUCLEAR MEDICINE & ALLIED SCIENCES

(Defence Research & Development Organisation)

Lucknow Road, Timarpur, Delhi – 110054

CERTIFICATE

This is to certify that the project entitled "***Modelling, Simulation and Testing of a Few Polarizer Components Developed at INMAS, DRDO***", completed by Mr. Anto Augusty, a student of M.Tech., Nuclear Science and Engineering of Applied Physics Department at Delhi Technological University, New Delhi, embodies the original work carried out by him under my supervision and guidance. His work has been found very well for the partial fulfilment of the requirement of the degree of M.Tech.

It is further certified that, the student has developed the project during the period of 1st January, 2016 to 13th May 2016.

This report has not been submitted in part or full in any other University for award of any other degree.

Mr. Anto Augusty is a student of good moral character. I wish him success in future.

(**Mrs. Priyanka Sharma**)

Scientist 'C'

INMAS, DRDO

Delhi - 110054

Department of Applied Physics

Delhi Technological University (DTU)

(Formerly Delhi College of Engineering, DCE)

Govt. of NCT of Delhi

Bawana Road, Delhi-110042

CERTIFICATE

This is to certify that the Major project (AP-811) report entitled **"MODELLING, SIMULATION AND TESTING OF A FEW POLARIZER COMPONENTS DEVELOPED AT INMAS, DRDO"** *is a bonafide work carried out by Mr.* **Anto Augusty** *bearing Roll No.* **2K14/NSE/07**, *a student of Delhi Technological University, at* **INMAS, DRDO** *in partial fulfilment of the requirements for the award of Degree in* **Master of Technology** *in* "**Nuclear Science & Engineering**". *This is a copy right work of DRDO, Ministry of Defence and no part of this report/ study can be reproduced anywhere except for the purpose of the student's viva.*

(**Dr. Nitin K. Puri**)   (**Prof. S. C. Sharma**)

Assistant Professor   Head of Department

Department of Applied Physics   Department of Applied Physics

Delhi Technological University   Delhi Technological University

Delhi-110042   Delhi-110042

Candidate Declaration

I, hereby declare that the work which is being presented in this thesis entitled "***<u>Modelling, Simulation and Testing of a Few Polarizer Components Developed at INMAS, DRDO</u>***" is my own work carried out under the guidance of Dr. N. K. Puri, Assistant Professor, Department of Applied Physics, Delhi Technological University and Mrs. Priyanka Sharma, Scientist 'C', Institute of Nuclear Medicine & Allied Sciences, DRDO, New Delhi.

I further declare that the matter embodied in this thesis has not been submitted for the award of any other degree or diploma.

Date: Anto Augusty

Place: New Delhi   2K14/NSE/07

Acknowledgement

Firstly, I would like to thank Mrs. Priyanka Sharma, from the NMR department of INMAS, DRDO, who has guided me throughout the project. Her enthusiasm for science has been my motivation till the end. Her knowledge of the subject and her innovative ideas has been a great resource and inspiration. It was because of her constant guidance that I was able to complete this work.

I would never have the energy to work at INMAS if it were not for my post graduate mentor and supervisor Dr. Nitin K. Puri. It was the fundamentals that he taught me that enabled me to understand the problems that I faced during my project. He always had time to spare for me and guide me through the right path. He was the one who taught me to have a research oriented approach to my learning. He always inspired me to be well updated in anything that I am learning.

I would like to thank Prof. S. C. Sharma, Head of Department, Applied Physics, Delhi Technological University for recommending me to work in an esteemed institute like INMAS. Without him I would never have been able to do a project like this in the first place. His energy and youthfulness has always made me challenge myself and be devoted to the work I am doing. His smiling face has always been a great comfort whenever I used to be tensed or worried.

I would like to thank Dr. Subash Khushu, Head of Department of NMR Department, INMAS, for giving me the opportunity to work in INMAS. It was a great experience for me and has given me a whole new perspective to learning. His knowledge and hardworking nature has been a source of great inspiration to me.

Finally, I am thanking my parents and all my friends for their support and encouragement. They have been with me even in difficult times. Their advice and support is something that has always kept me going. They are the ones who have always given smiles in my life. I am always grateful to them.

Anto Augusty

2K14/NSE/07

Abstract

A proton MRI is usually used to image the human body. It works by detecting the signal from the hydrogen atom present in the human body. Since majority of the human body is made up of water molecules, the signal received by the MRI is of sufficient strength and can be analysed. But this is not the case with organs that does not has any presence of water molecules like the lungs. For such organs it is impossible to get images of sufficient clarity using the proton MRI. This is where hyperpolarized xenon MRI has importance. In a hyperpolarized xenon MRI, the patient is made to inhale hyperpolarized xenon and the signal from the noble gas is detected using the MRI. The signal from the hyperpolarized gas has an enhancement of the order of several thousand factors compared to thermally polarized gases. In this project we will be focussing on the modelling, simulation and testing of a few polarizer components developed at INMAS, DRDO.

Contents

List of Figures

Figure Name   **Page No.**

List of Tables

Table Name   **Page No.**

Units and Values

Here are the most used units and values in this thesis:

Gyromagnetic ratio (γ)	no units	
Magnetic field intensity (B)	Tesla	
Electron Larmor frequency (ω_{os})	radians/sec	
Nuclear Larmor frequency (ω_{0I})	radians/sec	
Temperature (T)	K	
Detuned frequency (δ)	sec^{-1}	
Wavelength (λ)	nm	
Bohr magneton (μ_B)	J.T^{-1}	9.274×10^{-24}
Permeability (μ)	H/m	
Permeability of free space (μ_0)	H/m	$4\pi . 10^{-7}$
Thermal conductivity (k)	W/(m.K)	

Chapter 1

Introduction

A polarizer was designed at INMAS, DRDO with the intention of producing hyperpolarized xenon for its use in NMR/ MRI applications. The polarized noble gas is produced by means of spin exchange optical pumping process. The experimental arrangement requires a high power laser system, an oven, an optical pumping cell, a Helmholtz coil, magnet arrangement for xenon accumulation, a glove box for rubidium handling.

For the polarization process the solid rubidium has to be first heated to vapour form and transferred to the pumping cell. Rubidium being a corrosive material has to be carefully handled and also precautions should be taken that the element is not oxidised lest it would be useless for the polarization process. The pumping cell is kept in an oven. The temperature inside the oven should be around $80 - 160℃$ for keeping the rubidium in its vapour form. The light entering the pumping cell must be circularly polarised for the optical pumping to take place. Also there should be a uniform and strong magnetic field of ~ 30 G for the Zeeman splitting of rubidium atoms. After the polarization process low temperatures and high magnetic fields of the order of ~500 G is required for xenon accumulation.

The aim of this project include understanding and operating the high power laser which include the procedures for its starting up and shutting down, testing the temperature inside the oven, testing the polarity of the light entering the pumping cell, modelling and testing the magnetic field inside the already present uni-axial Helmholtz coil, modelling and testing the magnetic field inside the magnet arrangement for xenon accumulation, modelling and simulation of a tri-axial Helmholtz coil for producing more homogeneous and strong magnetic field, modelling and simulation of linear Halbach array, Halbach cylinder and magnet arrangement consisting of four dipoles with an aim of providing a strong and uniform magnetic field for the accumulation of xenon, modelling and simulation of the temperature profile inside the pumping cell and the temperature profile inside the helical condenser coils.

Chapter 2

Review of Literature

2.1 Introduction

The NMR phenomenon has been widely used in several applications in the fields of physics, biology, chemistry and medicine. One of the important applications of this phenomenon is in Magnetic Resonance Imaging. The nuclear spin polarization has a very low value at thermal equilibrium. By using lower temperatures and higher magnetic fields, it could be increased a bit more but this would be costly. By using hyperpolarized noble gases having nuclear spin polarizations four or five orders higher than at thermal equilibrium as magnetic tracers, signals of sufficiently higher magnitude could be obtained.
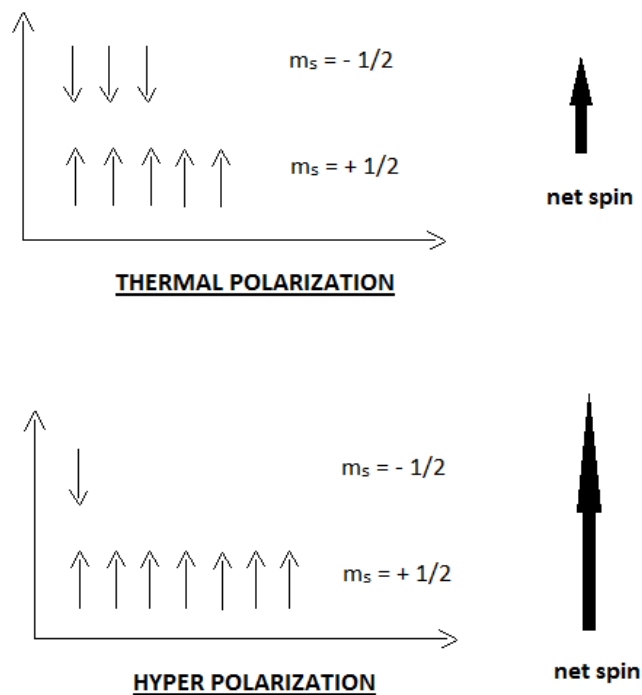
Fig 2.1: thermal polarization vs hyperpolarization [1]

This review surveys the various aspects of polarization of the noble gases. Section 2.2 deals with the basics of MRI, section 2.3 deals with the advances in the NMR/MRI, section 2.4 deals with the rubidium atom, section 2.4 deals with spin exchange optical pumping, section

2.5 deals with principles of optical magnetometry and section 2.6 deals with recovery of polarized xenon.

2.2 Basics of MRI

A proton MRI works by detecting the NMR signals from the hydrogen atom. A hydrogen atom can be compared to a compass needle. Suppose a compass needle is in a magnetic field, it will align itself in the direction of the magnetic field. The needle will come to rest after a few oscillations or vibrations. After coming to rest, if we give a push with another magnet in the perpendicular direction, then again the needle oscillates for some time and then again comes to rest. Usually the second magnet is a weak one and it does not have enough strength to push the needle against the primary magnetic field. But if we give a series of pushes in synchrony with the oscillation of the needle then ultimately sufficient force is attained to keep the needle oscillating.

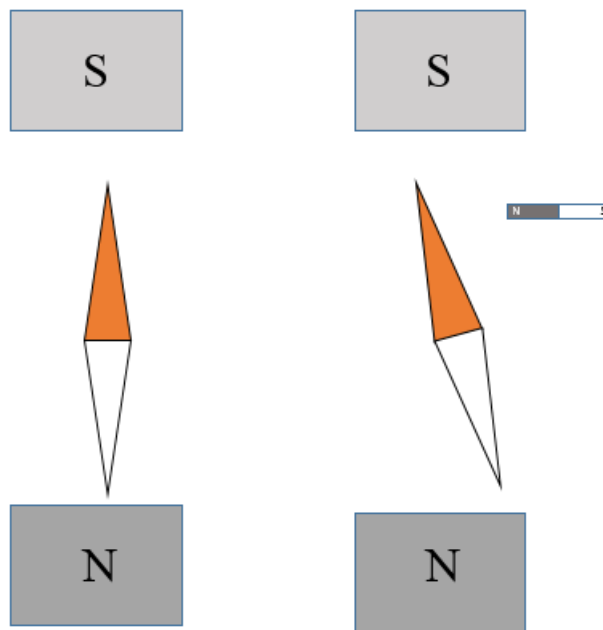Fig 2.2: push given by an external magnet

Now repeated pushes can be given by using an oscillating magnetic field. By passing alternating current to a coil gives an oscillating magnetic field. The frequency of current should be equal to the frequency of oscillation of the needle and this frequency is called resonant frequency. The oscillating magnetic fields are called radio waves. After the radio waves are

stopped, the needle oscillates with gradually decreasing amplitude. In this process, it gives off radio waves. The coil now acts as a receiver when the coil comes under the influence of the oscillating magnetic field or the radio waves, then current is produced which can be detected and analysed. This is the basic principle of the MRI.

Unlike the needle, the proton in the nucleus has a spin. In the presence of an external magnetic field, the proton starts pecessing around the magnetic field at a frequency known as the Larmor frequency.

$$f = \gamma B_0$$

Where γ is the gyromagnetic ratio of the material and B_0 is the magnetic field intensity. So these effects also should be considered. Now initially if we only consider the external magnetic field the precession of the spin can be shown as:
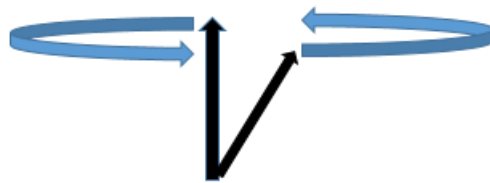
Now if resonant radio waves are transmitted perpendicular to the external magnetic field, the effect of it would be to induce precession around an axis perpendicular to the external magnetic field. Considering a rotating frame of reference, this can be represented as:
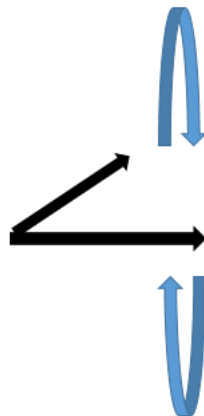
Collisions between nuclei give rise to magnetization constantly approaching the equilibrium size. This is called relaxation. The relaxation will occur in two different time scales. The magnetization perpendicular to the external magnetic field (transversal magnetization) decreases rapidly compared to the recovery of magnetization along the field (longitudinal magnetization).

We can control the contrast in an MR image by the choice of measuring method. We call an image T_2 weighted if the acquisition parameters are chosen so that the image contrast mainly reflect $T_2 -$ variations. The echo time, TE, is the period from which we rotate the magnetization till the time we measure the radio waves. Echo time can also be said as the period within the measurement which gives T_2 weighting in the images. The greatest sensitivity to T_2 variation will be achieved when TE is equal to T_2. Similar measurements is repeated several times, the time between these repetitions is called repetition time, TR. In the measurements, the longitudinal magnetization is rotated into the transverse plane and as the transverse component decreases, the radio waves are emitted. If we use the magnetization often (by taking short TR) then the signal received will be small whereas if we wait for longer time between repetitions (by taking long TR), then the signal is more as the magnetization will nearly recover to equilibrium between repetitions. If TR is longer than maximum T_1, the T_1 contrast will disappear. The transverse magnetization immediately following the rotation of the nuclei will reflect the equilibrium magnetization. Equilibrium magnetization is due to hydrogen concentration which is also known as the proton density (PD). A longer TR results in limited T_1 - weighting but a strong signal. For a shorter TR, the signal becomes more T_1 - weighted but will be less intense. Thus,

1. Short TR and short TE gives T_1 weighted images.
2. Long TR and long TE gives T_2 weighted images.
3. Long TR and short TE gives PD weighted images.

A "sequence" is an MR measurement method. A measurement is characterized by a sequence of events. In a spin echo sequence as shown in the figure below, the magnetization is first rotated 90° away from equilibrium using radio waves. Then due to field inhomogeneity, dephasing occurs. Then using radio waves, the magnetization is turned 180°. After some time, refocussing is done and then the signal is measured. The various elements of sequences are:

1. Excitation – it involves the turning of magnetization away from equilibrium

2. Dephasing – when the inhomogeneity in field causes nuclei to precess at different speeds. The alignment of the nuclei is lost and so the signal is lost.

3. Refocussing pulse – after excitation and dephasing, there is a loss of signal due to inhomogeneity. A part of this signal can be recovered by sending a 180º radio wave pulse. The nuclei which precess more rapidly during dephasing are pushed farthest and as they gradually align again, the lost signal is recovered by the "echo" measured.

4. Readout – it is the measurement of the MR signal from the body.

5. Waiting times – these are the periods wherein the relaxation contributes to the desired weighting.
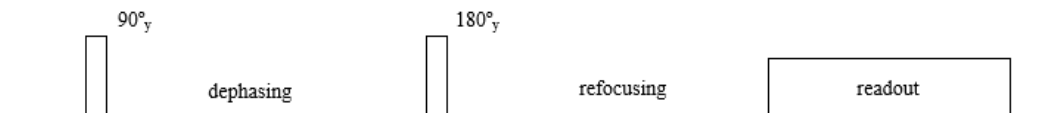
Fig 2.3: spin echo sequence

2.3 Advances in NMR/MRI using Hyperpolarized Noble Gases

Even though MRI is possible without using hyperpolarized spin states, the signal intensity achieved is very low. For good MRI resolution, gases with high spin concentrations, high gyromagnetic ratio and shorter longitudinal relaxation times are required. Hyperpolarization allows the use of gases with low concentrations and low gyromagnetic ratios. The Noble gases are polarized by making use of the optical pumping of alkali metals and the polarization is then transferred to noble gas nuclei by collisions or by the formation of van der Waal molecules. Various methods for producing hyperpolarized agents are dynamic nuclear polarization (DNP), para hydrogen induced polarization (PHIP), metastability exchange optical pumping (MEOP) and spin exchange optical pumping (SEOP).

2.3.1 Dynamic Nuclear Polarization

Overhauser proposed in 1953 that by saturating the electron paramagnetic resonance transition, it could be possible to transfer the large Boltzmann polarization of unpaired electrons to neighbouring nuclei. The signal intensities of NMR signals was enhanced by a

factor of $\frac{\gamma_e}{\gamma_l} \sim 660$ in the case of protons. Carver and Slichter later reported an experiment where they polarized [7]Li [2] and then [23]Na and ^{1}H nuclei [3] and achieved a signal intensity of ~ 100. This was the first demonstration of the dynamic nuclear polarization. Later DNP experiments were performed in solids and liquids. Hwang and Hill [4,5] and Kessenikh *et al* reported 9 GHz DNP experiments using systems with in-homogeneously broadened EPR spectra.

The polarization transfer mechanisms in a DNP experiment can be understood by considering the general static Hamiltonian for an electron nuclear system of the form:

$$H = H_S + H_I + H_{SI} = \omega_{0S}S_Z - \omega_{0I}I_Z + H_{SI}^{iso} + H_{SI}^{dip}$$

$$= \omega_{os}s_z - \omega_{0I}I_Z + A(S_ZI_Z + S_YI_Y + S_XI_X) + BS_XI_Z \qquad [6]$$

Here, ω_{os} is the electron Larmor frequency, ω_{0I} is the nuclear Larmor frequency, S_i is the electron spin operator, I_i is the nuclear spin operator. H_{SI}^{iso} represents the isotropic hyperfine interaction between electron and nucleus. H_{SI}^{dip} is anisotropic dipolar coupling. H_{SI} represents hyperfine coupling, the secular and pseudo secular hyperfine interactions are denoted by the coefficients *A* and *B*.

Overhauser effect is a DNP mechanism that requires the presence of relaxation processes which can simultaneously flip an electron and a nuclear spin. In liquids it is based on time dependent dipolar and scalar interactions between the nuclei and the electrons. In solids Overhauser effect requires mobile electrons such as in the conduction band of metals [2]. DNP processes are most efficient at low temperatures. The implementation of the DNP experiments requires a microwave source, a waveguide to transmit microwaves from source to NMR probe and also multiple frequency NMR probe with waveguide in order to irradiate the sample. Initially, the main application of the technique was to perform experiments at low temperatures for producing polarized targets for investigating the spin dependence of nuclear forces in experiments relate to scattering.

## 2.3.2 Para Hydrogen Induced Polarization

PHIP is a method which is applied to small molecules so that the MR imaging signal is enhanced. Here para-hydrogen is used to introduce large nuclear polarizations into proton spin levels. PHIP involves transition metal catalysed hydrogenation reactions involving the use of para hydrogen enriched samples of hydrogen as reactant. Seldler *et al* 1983, Bowers and

Weitekamp, 1986, 1987 observed the first instance of PHIP in an NMR experiment while they were investigating a hydrogenation reaction. The existence of two hydrogen nuclear – spin isomers, in ortho and para state was demonstrated by Paul Harteck and Karl – Friedrich Bonhoeffer by cooling hydrogen and determining the thermal conductivities of para- and ortho hydrogen. Para hydrogen was first used for hyperpolarization applications in NMR in 1983 [7]. The experimental proof of PHIP effect was accomplished in 1987 [8, 9]. This method has the advantage that para-hydrogen can be produced with less costs. The design of molecules hyperpolarized with para-hydrogen could have a huge impact in the area of contrast agents. By using in combination with remote detection technologies, gas flow behaviour in reactors could be monitored very efficiently. This can help increase the understanding of chemical reactors.

2.3.3 Metastability Exchange Optical Pumping

Here helium-3 is polarized. Optical pumping is carried out at standard conditions and at low pressure and low magnetic fields. In this method, first optical pumping is performed on metastable state 2^3S of helium-3 atoms and then transfer of nuclear orientation to ground state takes place through metastability exchange collisions. To date, MEOP has been applied to helium-3 and a polarization of up to 90% could be achieved. The MEOP process is a much faster process compared to SEOP process. Also ^{129}Xe that is hyperpolarized using SEOP process has lower signal in lung imaging compared to hyperpolarized ^3He from MEOP process. One of the drawbacks of this process is the compression of the gas after the process. Dedicated compressors are to be designed for this purpose.

For the MEOP process, direct pumping of helium-3 from the ground state is not possible due to the high energy difference between 1^1S_0 and 2^3S_1 states. So, inside the pumping cell, a weak rf discharge is sustained in order to populate higher states of helium. Then, a small fraction of the molecules fall into the metastable state 2^3S_1. Now, this state will not decay via photon emission due to forbidden transition between singlet and triplet states and angular momentum conservation rule. The optical pumping is then performed using circularly polarized light that is tuned at 1083 nm on the transitions between 2^3S_1 and 2^3P sublevels. Then isotropic radiative de-exitation happens and atoms at 2^3P state come back to metastable state. Then metastability exchange collisions happen between ground state atoms and polarized metastable helium-3 atoms. Finally there is a transfer of nuclear orientation from metastable state to ground state that is more populated [Nac85] [Cou02].

$$3He + {}^3He_\uparrow^* \rightarrow {}^3He^* + {}^3He_\uparrow$$
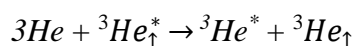
2.3.4 Spin Exchange Optical Pumping

This technique is based on the transfer of angular momentum in photons to the electron spins in an alkali metal and then the transfer of polarization from the electron spins to nuclear spins of a noble gas. In this process, a circularly polarized pump light is absorbed by alkali metal vapour that is contained inside a glass cell. After the alkali metal is polarized, the cell is then filled with large quantity of noble gas and then due to collisions electron spin polarization is transferred to the nuclei of the noble gas. There are a lot of limitations in achieving a large polarization in the noble gases. For high polarization in noble gas to happen there should be high polarization in alkali metal. The alkali spin relaxation affects the alkali metal vapour polarization. This is mostly due to the alkali-alkali collisions. After the polarization is transferred to xenon, xenon spin relaxation due to collisions further affects the polarization value. After the polarization of xenon is complete, further work is required for the accumulation of the hyperpolarized noble gas and also to remove the alkali vapour from gas mixture.

Spin exchange optical pumping process using rubidium as the alkali metal is briefly explained as follows. There are rubidium vapours in the pumping cell. It is placed in a magnetic field. The magnetic field is produced by a Helmholtz coil. A mixture of Xe, N_2 and He_4 gas is then pumped to the pumping cell. Nitrogen is added to the pumping cell to quench radiative de-excitation of the alkali metal which is a source of rubidium depolarization due to relaxation with its nuclear spins. When overall high pressure is needed, using only nitrogen is less efficient, so He_4 is also added.

Circularly polarized light is used to optically pump the rubidium atoms. The light from the laser is unpolarised. It is made linearly polarized using the polarizing beam splitter cube which converts the unpolarised light into linearly polarized light. There will be two linearly polarized light, one whose polarization is in the x direction and other whose polarization is in the y direction. The linearly polarized light in the y direction is made to incident on the quarter wave plate at an angle of 45º to produce circularly polarized light. The light is made to incident at 45º because only then both the x and y component of the incident linearly polarized light will be equal in magnitude and the 90º phase shift provided by the quarter wave plate to one of the component causes the light to be circularly polarized. It is this circularly polarized light that will be used to pump the rubidium atoms. The light passing out from the pumping cell as well as the light coming out from the polarizing beam splitter cube that was polarized in the x direction will be directed to a beam dump. The frequency of the pump beam is equivalent to

the D1 frequency line of the rubidium atoms. A probe beam which is slightly detuned from the D1 frequency to prevent the pumping of the atoms in that direction is used to quantify the degree of polarization in rubidium.

2.3.4.1 Optical Pumping

Right circularly polarized light has the notation 'σ+' and the left circularly polarized light has the notation 'σ-'. We will be using right circularly polarized light in our experiment. The wavelength of the laser used will be corresponding to the transition between $5^2s_{1/2}$ and 5 $^2p_{1/2}$ which is called the D1 transition line of the rubidium atoms and is equal to 794.7 nm. The magnetic field causes a small energy splitting between the mf states in that direction. The 'σ+' polarized resonant light can cause +1 shifts in the m_f states ($\Delta m_f = +1$) along the axis of propagation. So it is necessary to apply a magnetic field parallel to the magnetic field to observe optical pumping. The decay back to the ground state will have an average $\Delta m_f = 0$. After a few milliseconds a large portion of the electrons will be in the maximal m_f state and it will no longer absorb photons. Now it is said to be polarized.
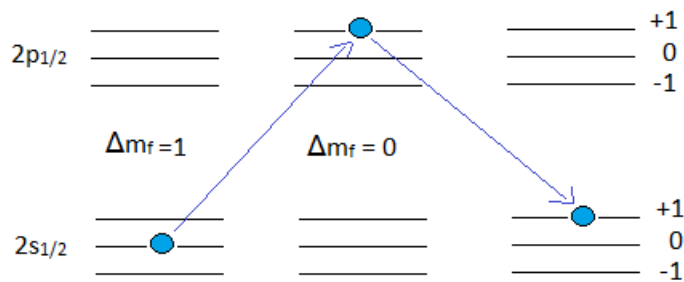
Fig 2.4: schematic representation of optical pumping process

2.3.4.2 Spin Exchange

By optical pumping the alkali metal is polarized. Now by spin exchange the polarization of any compound (nuclear spins) present in the pumping cell is affected the spin exchange cross sections are dependent on the molecular interaction between the foreign compound and the alkali metal which can either be simple two body hard core collisions or three body collisions leading to the intermittent creation of alkali metal – foreign compound van der Waals molecules.

2.4 Rubidium Atom

Rubidium is present in the first column of the periodic table. They have only one valence electron and thus similar to hydrogen atom. Its two common isotopes are ^{87}Rb and ^{85}Rb. Rubidium configuration:

$$1s^2 2s^2 2p^6 3s^2 3p^6 3d^{10} 4s^2 4p^6 5s^1$$
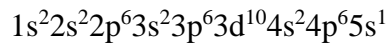
The energy levels are noted as $^{2s+1}l_j$. Here 's' is the spin of the electron, 'l' is the azimuthal quantum number and 'j' is the total angular momentum and is given by (l+s). 'l' has values 0, 1, 2, 3…which is denoted as s, p, d, f…The levels are named by their energy quantum number 'n' and the orbital angular momentum 'l' and the notation is 'nl', where n is 1,2,3…Since optical pumping is a precise phenomenon, so to understand it we have to consider more finer energy levels.

Now j = (l+s) is the total angular momentum for single electron atom. It has range from |l-s| to |l+s|. From the point of view of the electron the nucleus is a positive charge moving around it. The interaction of nucleus with electron gives the new angular momentum F which is equal to (I+j) where I is the nuclear spin. The value of I is 5/2 for ^{85}Rb and is 3/2 for ^{87}Rb. F has Eigen values in the range of |I-j| to |I+j|. This is called hyperfine structure.
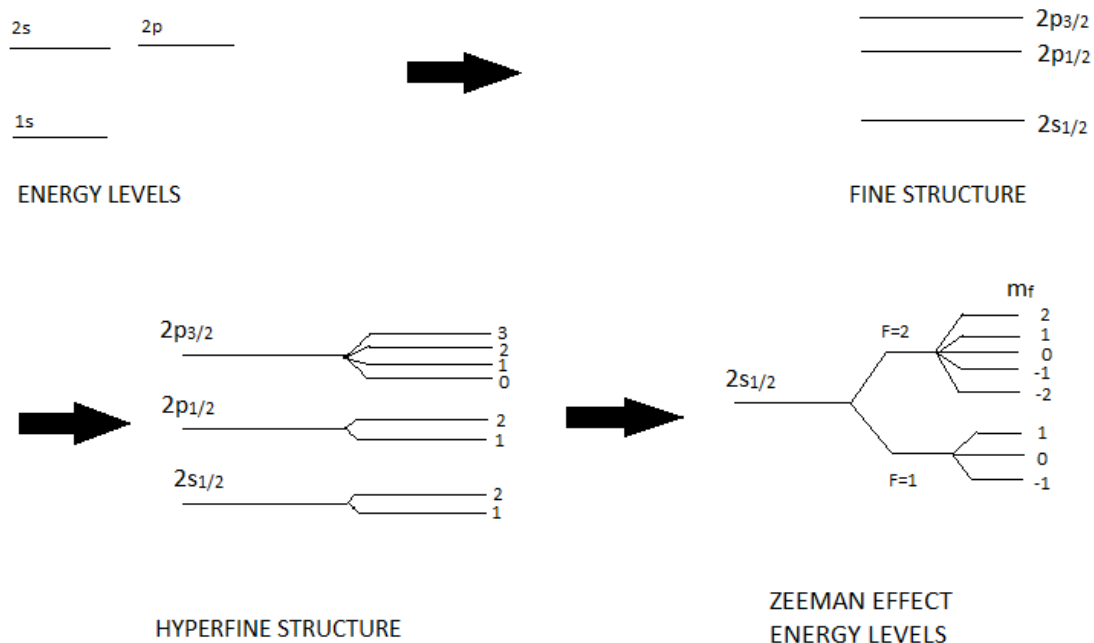

Fig 2.5: energy levels in ^{87}Rb

Now if there is an external magnetic field further splitting of the energy levels happens and this is called the Zeeman Effect. The splitting energy depends on the projection of F in the direction of B which will be called 'M'. The range is $-f < m_f < f$.

2.5 Properties of Noble Gases that makes it Relevant for MR Applications

2.5.1 General Properties

The three phases of xenon can be attained in laboratory conditions. It is gaseous at standard temperature and pressure. It can easily be liquefied (boiling point: 165.1 K at 1 atm) and frozen (melting point: 161 K at 1 atm). For hyperpolarization applications, xenon is mostly used in its gaseous form. Experiments are also conducted with its liquid form (Fitzgerald *et al* 1998, Tseng *et al* 1999), with frozen (Gatzke*et al* 1993, Bowers *et al* 1993, Augustine *et al* 1998) and with supercritical xenon (Haake*et al* 1998, Leawoods*et al* 2000). Xenon is an efficient solvent in its liquid and supercritical phase with densities higher than the gas phase (Rentzepis and Douglass 1981, Leawoods*et al* 2000).

The atomic number of xenon is 54 and its atomic mass is 131. It has nine naturally occurring isotopes with masses ranging from 124 to 136. Seven are stable and two are radioactive with long lives (^{124}Xe and ^{136}Xe). The isotopes ^{129}Xe and ^{131}Xe are both stable and NMR active. The gyromagnetic ratio of ^{129}Xe is about four times higher than ^{131}Xe leading to a much higher sensitivity.

2.5.2 Solubility

In terms of Ostwald coefficient solubility is the ratio of volume of gas at its partial pressure in the liquid to the volume of the absorbing liquid. By this definition the solubility of xenon is high for organic solvents. The mole fraction solubility x_1 is given by the ratio $x_1 = n_g/(n_g+n_l)$ where n_g, n_l are the number of moles of gas and liguid at the same temperature and gas partial pressure (1 atm). The temperature dependence of x_1 of Xe in water in the temperature range 273 – 353 K is given by the empirical formula (Clever 1979):

$$\ln(x_1) = -74.7398 + 105.210/(T/100 \text{ K}) + 27.4664\ln(T/100 \text{ K})$$

The xenon solubility in blood depends not only on the temperature but also on the level of oxygenation. Due to its hydrophobic nature, being electrically neutral and non-polar, it has only limited solubility in water. The liquid water is macroscopically connected random network of hydrogen bonds which constantly reorganizes themselves (Stillinger 1980). The water

molecules will rearrange themselves around the non-polar molecule in a convex hydrogen bond polyhedron of a size large enough to accommodate the solute. The low solubility of non-polar molecules in water compared to organic liquids can be understood on the basis of molecular dynamics simulation of distribution of cavities in hexane and water.

2.5.3 Anaesthesia

This property of xenon makes its use in MR applications very interesting. The first use of xenon as anaesthetic was reported in 1946 and it was used on a mice (Lawrence *et al* 1946) it produces anaesthetic effects in humans at MAC values of 71% atm (Cullen *et al* 1969). Its advantages as an anaesthetic agent are: it is non-teratogen, it does not deplete the ozone layer, it offers good circulatory stability, does not influence body temperature, has better regional perfusion of individual organs and has rapid washout (Marx *et al* 2000). The target sites of anaesthetics are either the lipid portions of neural membranes or the hydrophobic pockets in certain crucial excitable proteins (Franks and Leib 1994).

The relation between anaesthetic potency and lipid solubility was first reported and published by Meyer (1899). Two years later a similar theory was published by Overton (1901). Mayer and Overton had found a nearly linear relation between potency and partition coefficient of many types of molecules. Attempts were made by Miller *et al* (1981) to investigate the site of anaesthetic action based on chemical shift of xenon in biological systems such as lipid bilayers, bio membranes and myoglobin.

2.5.4 Availability

There is a sufficient amount of xenon in the Earth's atmosphere (concentration 0.087 ppm). Even though it is cheap at present but its demand may increase in the coming years as it is finding applications in various fields of science and engineering.

2.5.5 Chemical shift

When a bare nucleus in vacuum is subjected to an external field then its Larmor frequency will differ from that of the nucleus surrounded by its electrons and the rest of the medium. This is called chemical shift, σ. The electrons from the electron cloud precesses around the applied magnetic field. The field produced by the electrons opposes the applied field. The external field polarizes the electronic shells thereby producing an additional magnetic and electric field at the nucleus. Larger polarizability of xenon compared to other

noble gases means that xenon can be expected to have higher interactions with its environment but it will be not chemically or structurally disruptive (Rentzepis and Douglass 1981). Xenon has chemical shift range of around 350 ppm in solution and more than 7000 ppm in compounds.

An observation in Meersman and Haake 1998 also illustrates the high polarizability of the xenon cloud. Polarizability also plays an important role in xenon binding to protein and transport through protein interior. The chemical shift is an NMR property that is much easier to measure compared to the relaxation times. The sensitivity of the chemical shift of xenon has found a wide range of applications. Xenon has a chemical shift of 240 ppm in its liquid phase and about 300 ppm in the solid phase. The range of chemical shifts and longitudinal relaxation rates in liquid and gaseous states of xenon were studied by Streever and Carr (1961) and then Hunt and Carr (1963). The observations they made showed that the chemical shift is accurately proportional to density over a range from rarefied gases to the liquid phase. The spin rotation coupling plays an important role in explaining the chemical shift and relaxation of xenon.

The study of chemical shift in xenon gas was also done by Jameson and his collaborators (Jameson *et al* 1970, 1973). In the gas phase, the chemical shift is due to the collisions between xenon atoms and it is dependent on the pressure and temperature. Xenon helps in the study of water structures due to its hydrophobic properties. Both the thermally polarized as well as hyperpolarized xenon has been used for various studies which allowed resolution of the dynamics of formation of ordered, cage like structure of water molecules (Ripmeester and Ratcliff 1990, Pietrab*et al* 1995). Such ordered structures are also the causes for the self-diffusion of water. The high sensitivity of chemical shift of xenon allows the use of functionalised xenon as a biosensor (Spence *et al* 2001).

2.5.6 Exchange between Sites

The large range of xenon chemical shift also helps in the study of exchange between sites. Transverse relaxation times contain the kinetic information about the exchange. Transverse relaxation times can be found by studying the resulting line shapes. By observing the line shapes and their dependence on various parameters such as field strength, temperature and concentration, information about properties characteristic to each environment and the exchange between them can obtained. (Pietrab and Gaede 1995, Springuel – Huet*et al* 1999).

Consider a two site model, A and B. Each site has its own population P_A and P_B, its chemical shifts v_A and v_B, residence time τ_A and τ_B and intrinsic transverse relaxation time T_{2A}

and T_{2B}, respectively. Depending on the chemical shifts and the exchange rates, the process can be slow, intermediate or fast exchange. In slow exchanges, a separate line is obtained for each site. Here $\Delta\omega = 2\pi\Delta v$ is the chemical shift difference between the states and τ is the average residence time of the state and equals the inverse of the exchange rate $\tau = k_{ex}^{-1}$. The linewidth of each resonance is given by:

$$\pi\Delta v_i = (1/T_{2i}) + (1/\tau_i)$$

As the exchange rate increases, the linewidth also increases reaching a maximum where the two lines merge into a single broad one.

2.5.7 Relaxation Times

A long longitudinal relaxation time for the isotope ^{129}Xe in gaseous form was observed by Proctor and Yu (1950) and its magnetic moment was measured using NMR techniques. Data on the T1 values of xenon gas were also provided by Brun*et al* (1954a, 1954b). He noted that the relaxation time of ^{129}Xe was much shorter than expected from dipolar interactions alone. A more detailed information about the relaxation behaviour of xenon was gained from the studies of Streever and Carr 1961 and Hunt and Carr 1963. The authors dicussed the possible relaxation mechanisms and on the basis of the measured dependence on density, concluded that the dominant contribution for the chemical shift was provided by the fluctuating magnetic field sampled by the spin during atomic collision. A study by Moudrakowski*et et al* (2001a, 2001b) investigated about the longitudinal relaxation of thermally and also laser polarized ^{129}Xe as a function of temperature. The main mechanism for relaxation at higher densities was later confirmed to be spin rotation. A study by Chann et al (2002) identified that the spin-rotation coupling within bound between Xe-Xe Van der Waals molecules as primary relaxation process at below 14 amagat densities.

Using polarized xenon and then measuring the relaxation times as a function of gas composition in mixtures of Xe with Ar, N_2 and He, an increase in relaxation time was observed with increasing buffer gas density ratio. For higher densities, binary relaxation times becomes important. The relaxation in liquid xenon was first studied by Hunt and Carr (1963). They obtained values around 16 min, independent of field and at temperatures in the range of -72 to 10º C. the relaxation studies of solid xenon were performed by Yen and Norberg (1963). They investigated the transverse relaxation time in Xe in ice as well as in liquid form and also its dependence with temperature. The authors measured a T2 value of 1 ms for xenon in ice form

at 4.2 K. it represents the pure dipolar rigid lattice relaxation time. Tseng *et al* (1999) measured relaxation in polarized liquid xenon at a field of 4.2 T and a temperature of 166 K.

2.5.8 Diffusion

The diffusion coefficient of gases are higher than that of liquids. The resolution of the MR images are affected by the typical diffusion length of the gas in the system under study. The knowledge of diffusion coefficients is important for imaging experiments. The large diffusion distances of gases allow a unique probe into the structures of porous systems (Mair*et al* 1999, Mair and Walsworth 2002). Liquid diffusion in such materials allows to probe the structures on a scale below $50 - 100$ μm and helps in extracting information about the pore size and surface to volume ratios (Butler *et al* 2002). The diffusion coefficient of thermally polarized xenon at room temperature was 0.051 cm^2 s^{-1} (Peereboom*et al* 1989). Peled*et al* (1999) measured the diffusion coefficient of hyperpolarized xenon gas at 3 atm and 90 ºC to be 0.0193 cm^2 s^{-1}.

2.6 Principles of Optical Magnetometry

When light travels through materials that are dichroic and placed in an axial magnetic field, then a slight rotation of its plane of polarization will be observed. This phenomenon is called Faraday Effect. If the magnetic field strength is B, the length of the cell containing the material is L, then the rotation is given by,

$$\Delta\Phi=VBL$$

Where V is the Verdit constant of the material.

Now the superimposition of two linearly polarized light with a phase shift of 90º gives circularly polarized light. Similarly you can consider a linearly polarized light as a combination of a right circularly polarized and left circularly polarized light. At a certain level of superimposition when both the right and the left circular components are additive, we get a linearly polarized light in x direction and when the superimposition is subtractive, then we get a linearly polarized light in the y direction. Now at varying levels of superimposition, we get linearly polarized light in different directions. Different levels of superimposition is obtained when the right and left circularly polarized components travel in different speeds in the medium.
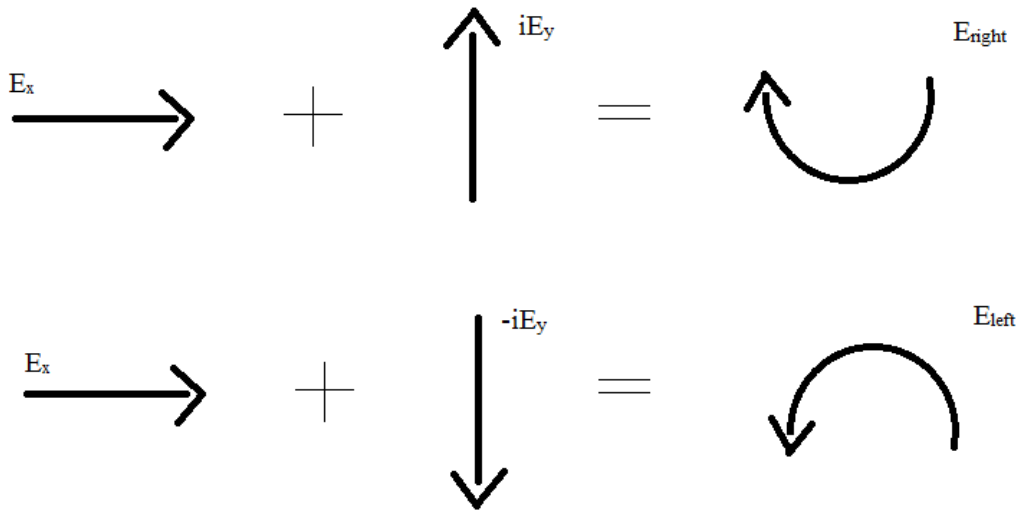
Fig 2.6: components of circularly polarized light

Unpolarised light comes from the laser. The polarizing beam splitter cube transmits linearly polarized components of the incident light. The light linearly polarized in y direction is incident on the pumping cell and the light polarized in x direction is directed to beam dump. The Helmholtz coil gives the necessary axial magnetic field. Now the initial direction of propagation of light is checked using the polarizer and photodiode, without filling the pumping cell with the gases and before switching on the magnet. Then again after filling the pumping cell and switching on the magnet and optically pumping the gas inside the cell with circularly polarized light, the direction of polarization in the probe beam is observed. The polarizer in its initial position will show lesser intensity. Then it is rotated till maximum intensity is obtained. The amount of rotation of the polarizer will give the amount of rotation undergone by the polarization plane of the light. The intensity of light is measured using the photodiode.

What happens inside the pumping cell is as follows. The pumping light which is right circularly polarized aligns the spins in the direction of propagation of the light. Now the current in the coil is such that the axial magnetic field is in the direction of propagation of light. When the direction of spin is in the direction of the magnetic field, then it is in the low energy state. Now as the magnetic field is applied the spins starts precessing around the magnetic field. Now the probe beam which is linearly polarized is made to pass through the pumping cell in the direction of the axial magnetic field. The component of spin in the direction of magnetic field

makes the material dichroic. As we have discussed, the linearly polarized light is a combination of left circularly polarized light and right circularly polarized light. Now when this light is incident on the material whose electron are spinning around its own axis and precessing around the magnetic field, the component of light that is rotating in the direction of the spin will experience a different index of refraction compared to the component that is rotating opposite to the spin. So the right circular component travels at a different speed compared to the left circular component and ultimately there is a rotation of the linearly polarized light. This rotation is proportional to the degree of polarization in rubidium.

2.7 Quantification of Rubidium

After the optical rotation is measured using a photo detector, the rubidium density and polarization can be calculated using the following formulas [10]:

For rubidium density:

$$n_{Rb} = \frac{8\pi(\Delta\emptyset)\delta^2}{L\Gamma\lambda^2\mu_B B}$$

Where n_{Rb} is the rubidium density, $\Delta\emptyset$ is the amount of rotation, L is the length of the pumping cell, δ is the detuned frequency of the laser, λ is the rubidium D1 wavelength of 794.7 nm, Γ is the rubidium D1 natural linewidth, μ_B is Bohr magneton and B is the applied magnetic field strength.

Now rubidium polarization can be calculated using the formula [10]:

$$P_{Rb} = \frac{56\pi(\Delta\phi)\delta}{3n_{Rb}L\Gamma\lambda^2}$$

2.8 Recovery of Polarized Xenon

Xenon is recovered by bringing the temperatures below 170K when only xenon solidifies and nitrogen and helium are evacuated to a pump. The xenon is purified and concentrated as a solid. The alkali metal also gets condensed at a slightly higher temperature than that of xenon.

Condensation can cause large decrease of magnetisation level. But in the presence of a magnetic field larger than 0.05T, the relaxation times can be large. Thus the polarization can

be maintained. Thus the xenon self-relaxation in solid phase is long only at very low temperatures and high magnetic fields.

2.9 Quantification of Xenon

After hyperpolarized xenon is separated from rubidium and other gas mixtures and stored in a phantom, it is taken to the MRI machine. Firstly the signal intensity of the hyperpolarized xenon (S_{hp}) is measured. Then in a similar phantom, thermally polarized xenon is filled at a slightly higher pressure and its signal intensity (S_{th}) is measured. The normalized signal enhancement factor ε can be calculated as [11]:

$$\varepsilon = \frac{S_{hp} c_{th} p_{th}}{S_{th} c_{hp} p_{hp}}$$

Where c represent the xenon concentration in gas mixture (in %) and p represent pressure of gas mixture in both cases. Finally the achieved hyperpolarization is given by εP_{th}.

2.10 Conclusion

Already, NMR and MRI are low SNR methods compared to other methods of spectroscopy. By using hyperpolarized gases, researchers were able to further improve the SNR by several orders of magnitude. One of the interesting characteristic of using laser polarized gases is the enhanced signal strength that can be obtained without the need of strong magnets. The low field MRI using hyperpolarized gases has the potential to improve the cost effectiveness of the NMR for clinical applications. The laser polarized noble gases has also found applications in material research. The relaxation times are usually the most important considerations for in vivo applications. A lot of research regarding hyperpolarized xenon and helium has focussed on the lungs. A lot of developments has also been made in the field of carrier technology. Even more exiting advancements in this area of MR research can be expected in the near future.

Chapter 3

Report on the Present Investigation

3.1 Polarizer System Description

A typical polarizer comprises of the SEOP unit and the xenon transport and storage unit.
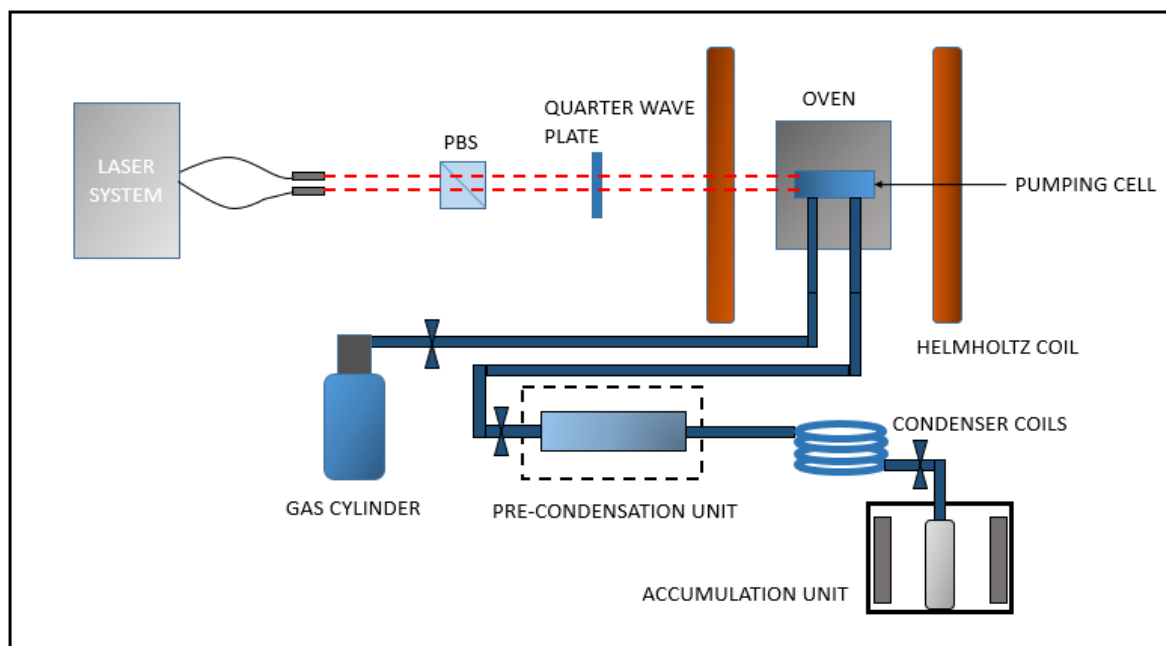

Fig 3.1: SEOP polarizer design

3.1.1 Optical Pumping/ Spin Exchange Unit

The SEOP unit consists of a laser system, a polarizing beam splitter cube, a quarter wave plate, a Helmholtz coil, an oven, a hot air blower and a pumping cell. The rubidium ampoule is heated in a glove box in inert environment and transferred using a pipette to the pumping cell. Special precautions need to be taken to prevent the oxidation of rubidium. The pumping cell is kept in the oven. To maintain the rubidium vapour density the oven has to be kept at a high temperature in the range 80 to 160℃. This is done by means of a hot air blower that constantly supplies hot air to the oven. A PID controller kept in the oven regulates the temperature. For optical pumping to take place, circularly polarized light is required. The light coming from the laser system is unpolarised. The unpolarised light is made linearly polarized

by means of a polarizing beam splitter cube and then it is made circularly polarized by means of the quarter wave plate. Once the rubidium is optically pumped the mixture of gases (Xe, N$_2$ and He) is passed into the pumping cell from a cylinder. Then the polarization from rubidium is transferred to xenon. Nitrogen and helium acts as quenching gases.

3.1.2 Xenon Transport and Storage Unit

After xenon gas is polarized, it is transported to a phantom through the condenser unit. To push the gases out of the cell, high pressure nitrogen gas is used. The gases are cooled using liquid nitrogen gas. First there is a pre-cooling unit, where all the rubidium gets solidified and gets separated. Then the gases pass through helical condenser coils. The helical arrangement provides maximum surface area for effective cooling. The gases then enter the phantom where xenon is solidified and the gases are pushed out. The phantom is kept in the magnet arrangement to prevent any loss of polarization of xenon. All the components are designed such that there are no contaminants such as paramagnetic materials. Xenon can be accumulated in batch mode or continuous flow mode.

3.2 Modelling and Simulation of the Polarizer Components

For the purpose of a better understanding of the working of polarizer system, the various components were modelled and simulated using COMSOL Multiphysics 4.3. For studying the uniformity and strength of the magnetic field through the pumping cell, the Helmholtz coil arrangement was simulated. A tri-axial Helmholtz coil arrangement was modelled which could provide even more homogeneous magnetic field between the coils. The pumping cell was simulated to study the heat transfer profile between the hot air inside the oven to the air inside the cell. A single turn in the helical coil arrangement was simulated for understanding the cooling mechanism of the hyperpolarized xenon through the condenser coils. Then, for the purpose of xenon accumulation strong and uniform magnetic fields are required. For this purpose, the magnet arrangement used in the polarizer was modelled. To produce even stronger and more uniform magnetic fields several magnetic configurations were designed and simulated which include a linear Halbach array, Halbach cylinder and a simple magnet arrangement using four dipoles.

3.2.1 COMSOL

COMSOL is a general purpose software platform. It is a useful tool for modelling and simulating physics based problems. Advanced numerical methods are used to find solutions

for the problems. It is a very flexible software and is very specifically designed for cross-disciplinary product development. There are several modules from which you can choose based on the type of application. For the complete overview of the model, you can refer to the model tree in the model builder window. It gives access to all the functionality such as geometry, mesh, physics, boundary, studies and visualizations. Other than the predefined equations, you can also include your own equations describing the property of the material, boundary condition, source etc.

Application specific modules can be added to your model that could give more modelling power by providing dedicated tools for mechanical, electrical, chemical and fluid flow applications. There are a set of core physics interfaces for various applications like laminar flow, structural analysis, electrostatics, pressure acoustics, heat transfer, electric currents and joule heating. For cases where preset physics option is not available, one could use the set of physics interfaces to set up simulations by defining equations. A set of templates for classical partial differential equations like Laplace's equation, wave equation, Poisson's equation, the Helmholtz equation, heat equation and convection diffusion equations are available.

A number of coordinate systems could be defined using COMSOL. Shortcuts are provided for the common coordinate systems such as cylindrical, rectangular, spherical etc. COMSOL makes it possible to work in 3D, 2D and 1D. Also 2D solutions can be mapped to a 3D surface or can even be extruded throughout a 3D volume. Tools for automatic and semi – automatic meshing are available in COMSOL Multiphysics. Also included are free tetrahedral and swept meshing. It has a combination of tetrahedral and boundary layer meshing for liquids and automatic tetrahedral meshing for physics defined in solids. You can also define a mesh sequence to take full control over the sequence of operations that are used for creating mesh. A number of primitive objects are available for geometry modelling. There are functions to extrude the general 2D geometry objects to 3D. There ae options for Boolean operations like union, difference and intersection that could be used to create more complicated shapes. All the geometric operations performed are organized as a series of operations in the Model Tree.

3.2.2 Modelling the Helmholtz Coil

A Helmholtz coil is a pair of identical circular coils whose distance between them is equal to its radius. This arrangement creates a uniform magnetic field between the coils. The

field components parallel to the axis gets added and the components perpendicular to the axis gets cancelled out. The various applications of this device include cancelling Earth's magnetic field, to generate magnetic fields in order to determine the magnetic shielding effectiveness, to calibrate magnetometers and navigational equipment etc.

The model in this simulation is built using 3D magnetic fields interface. Static currents and the fields are assumed. The magnetic vector potential A should satisfy the following equation [12]:

$$\nabla \times (\mu^{-1}\nabla \times A) = J^e$$

Where μ is permeability, and J^e denotes externally applied current density. The relation between magnetic flux density B and the magnetic field H is given by:

$$B = \nabla \times A$$

$$H = \mu^{-1}B$$

Since this model uses vacuum, the value of permeability is $\mu = 4\pi.10^{-7}\ H/m$. The value of the magnetic field intensity at the center is given by the formula:

$$B = \frac{8\mu_0 NI}{5^{3/2}a}$$

Where 'N' is the number of turns, 'a' the radius and 'I' the current.

Here the value of current is 5.2 A, the number of turns is 334, the radius of the coil is 36.6 cm.
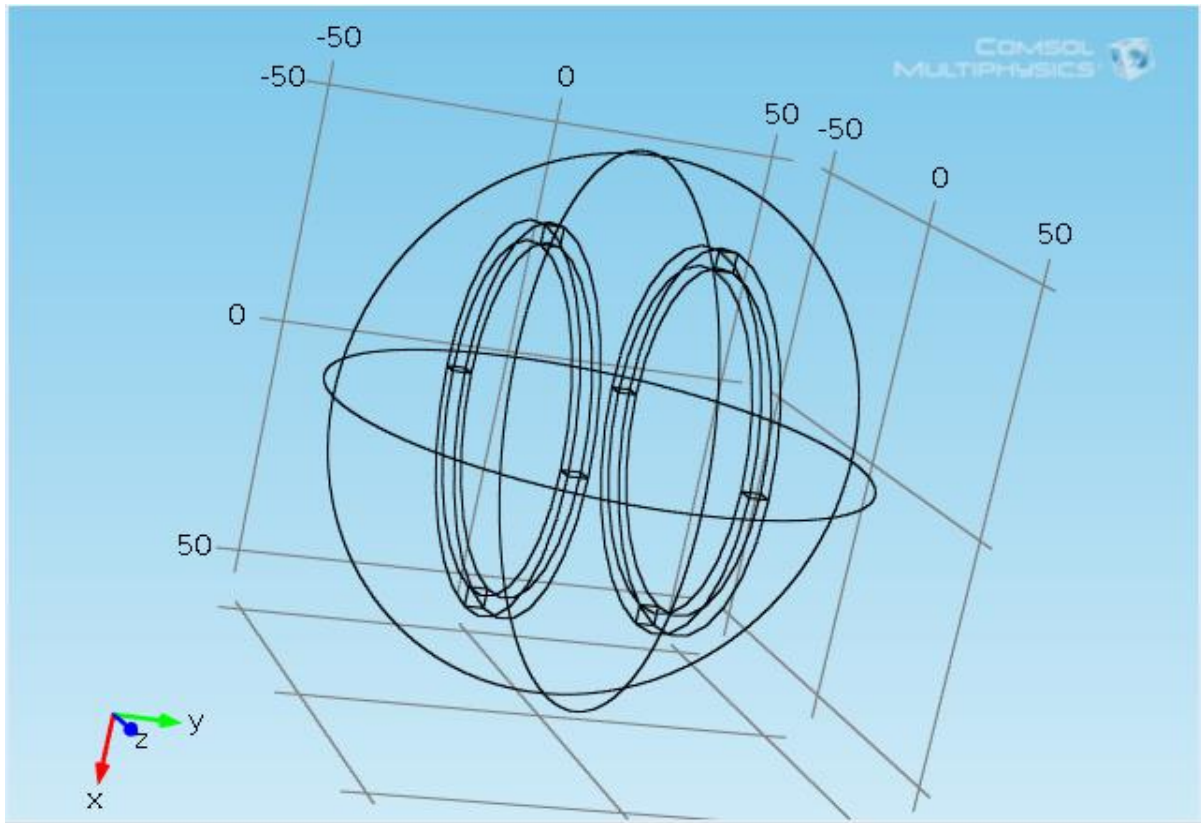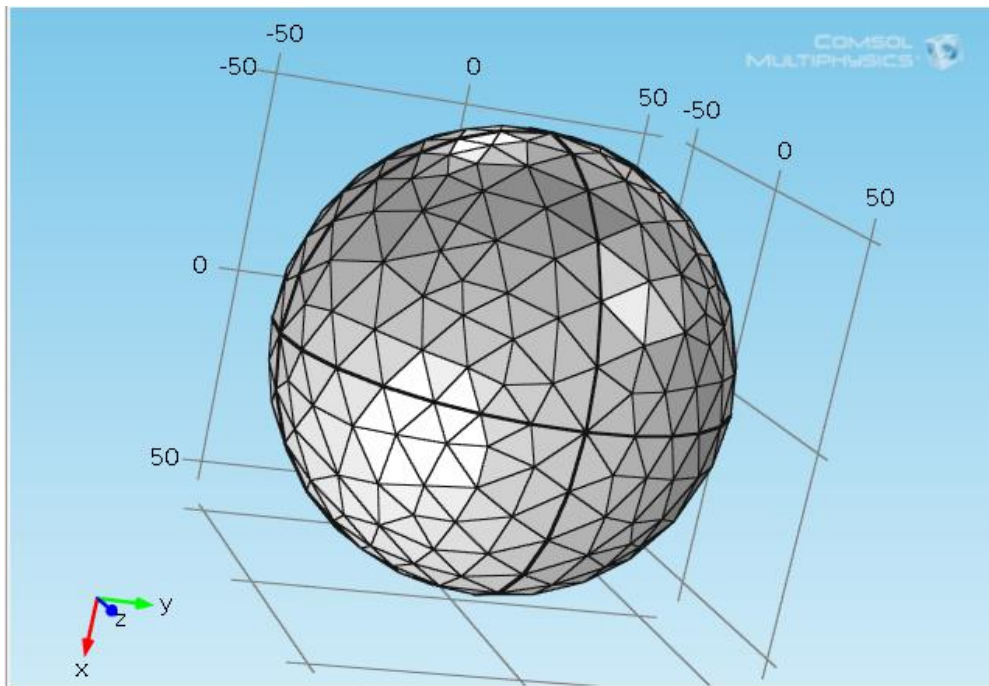
Fig 3.2: The 3D model

The magnetic fields (mf) subsection of the AC/DC module is selected for the simulation. The coil arrangement is modelled using the geometry tools. Firstly a work plane is defined in the xy plane. Thx y plane is defined at z=0 co-ordinate. Then in the plane geometry section two squares are placed, each representing a particular cross-section of the coil. Then the square cross-section is extended for an entire circle using revolve functionality thus completing the coil.

To model the surrounding air, the coil arrangement is encased in a big sphere. Then materials are defined for the coil and the air. For air, the value of relative permeability is given 1, relative permittivity is given 1, and various parameters like electrical conductivity, dynamic viscosity, ratio of specific heats, heat capacity at constant pressure, density and thermal conductivity are given by default. The coil material is defined as copper. For copper, an electrical conductivity of $5.998*10^7$ S/m is given, coefficient of thermal expansion is given a value of $17 * 10^{-6}$ 1/K, thermal conductivity is given a value of 400 W/m.K, Young's modulus is given a value of $110*10^9$ Pa and Poisson's ratio of 0.35.

The coils are defined as a multi turn coil in the magnetic field section. Each coil is defined separately as a domain. From the coil type, circular option was used. The constitutive relation for magnetic field is $B = \mu_0 \mu_r H$. The value of current is 5.2 A and the number of turns is 334. For specifying the direction of wires in the coil, a Reference edge sub feature is added and a group of edges forming a circle are selected. Then the software automatically computes the path of the wires from the geometry of the selected edges. The entire geometry is divided for computation using mesh command. The element size is chosen coarse and to get finer results free tetrahedral mesh arrangement is applied to the geometry.


The compute command is given and the results are plotted using the 3D plot group in the results subsection. The magnetic flux density and the flux profile in the xy plane is plotted. The Slice function is used to select the xy plane and Arrow volume is used to plot the magnetic field lines. Magnetic flux density is given in Tesla. The mf.normB expression is used to compute the flux density. The expression mf.Hx, mf.Hy and mf.Hz are chosen for plotting the field in x, y and z directions.
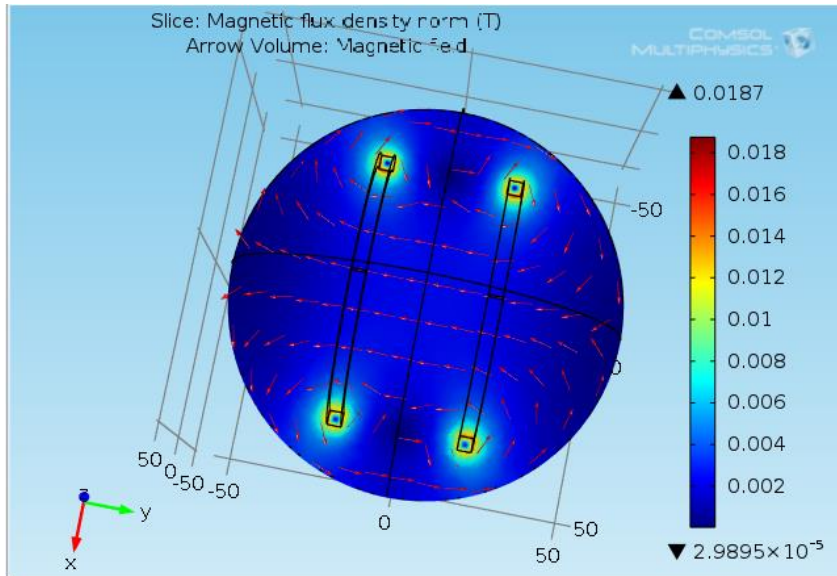
The value of magnetic fields at various points are:

SL.NO	X (CM)	Y (CM)	Z (CM)	VALUE (T)
1	-17.68611	-9.83341	-2.842e-14	0.00271
2	-14.57271	12.65434	1.421e-14	0.00268
3	-8.32417	3.38204	-1.42109e-14	0.00251
4	20.61595	-5.6783	-1.42109e-14	0.00242

In order to verify that the current path is properly computed, the coil direction variable for each coil is also plotted. The expressions mf.mtcd1.eCoilx, mf.mtcd1.eCoily and mf.mtcd1.eCoilz are chosen for the coil parameters in streamline1 and expressions mf.mtcd2.eCoilx, mf.mtcd2.eCoily and mf.mtcd2.eCoilz are chosen for the coil parameters is streamline2.
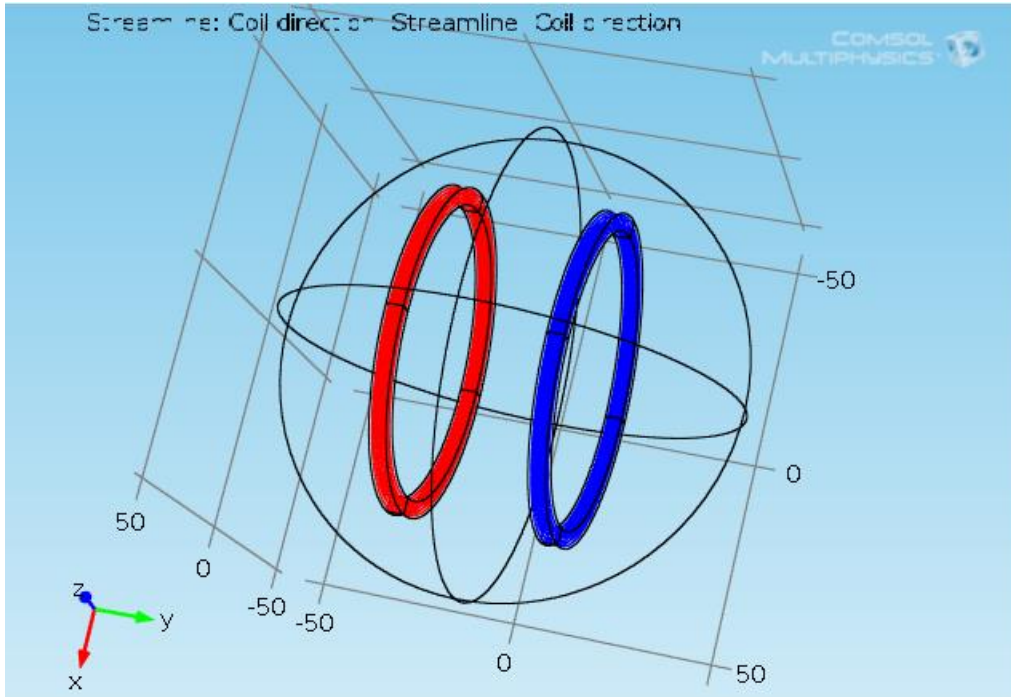
3.2.3 Modelling a Tri-Axial Helmholtz Coil

A tri-axial Helmholtz coil consists of 3 pairs of identical circular coils in each axis whose distance between them is equal to its radius. This arrangement creates a uniform magnetic field between the coils. The field components parallel to each axis gets added and the components perpendicular to the axis gets cancelled out. The coils are such that the inner edge of the middle coil is in contact with the outer edge of the inner coil and the outer edge of the middle coil is in contact with the inner edge of the outer coils. The current through each coil is controlled in such a way that the magnetic field produced at the centre by each coil is the same.

The model in this simulation is built using 3D magnetic fields interface. Static currents and the fields are assumed. The magnetic vector potential A should satisfy the following equation [14]:

$$\nabla \times (\mu^{-1}\nabla \times A) = J^e$$

Where μ is permeability, and J^e denotes externally applied current density. The relation between magnetic flux density B and the magnetic field H is given by:

$$B = \nabla \times A$$

$$H = \mu^{-1}B$$

27

Since this model uses vacuum, the value of permeability is $\mu = 4\pi.10^{-1}\ H/m$. The value of the magnetic field intensity at the center of any particular coil is given by the formula:

$$B = \frac{8\mu_0 NI}{5^{3/2}a}$$

Where 'N' is the number of turns, 'a' the radius and 'I' the current. The derivation to find the radius of the middle and outer coil is given in Appendix I. The number of turns in each coil is 334. The radius of first coil is 36.6 cm, the radius of second coil is 41.4 cm and the radius of third coil is 46.2 cm. The value of current through first coil is 5.2 A, the value of current through second coil is 5.88 A and the value of current through third coil is 6.57 A.
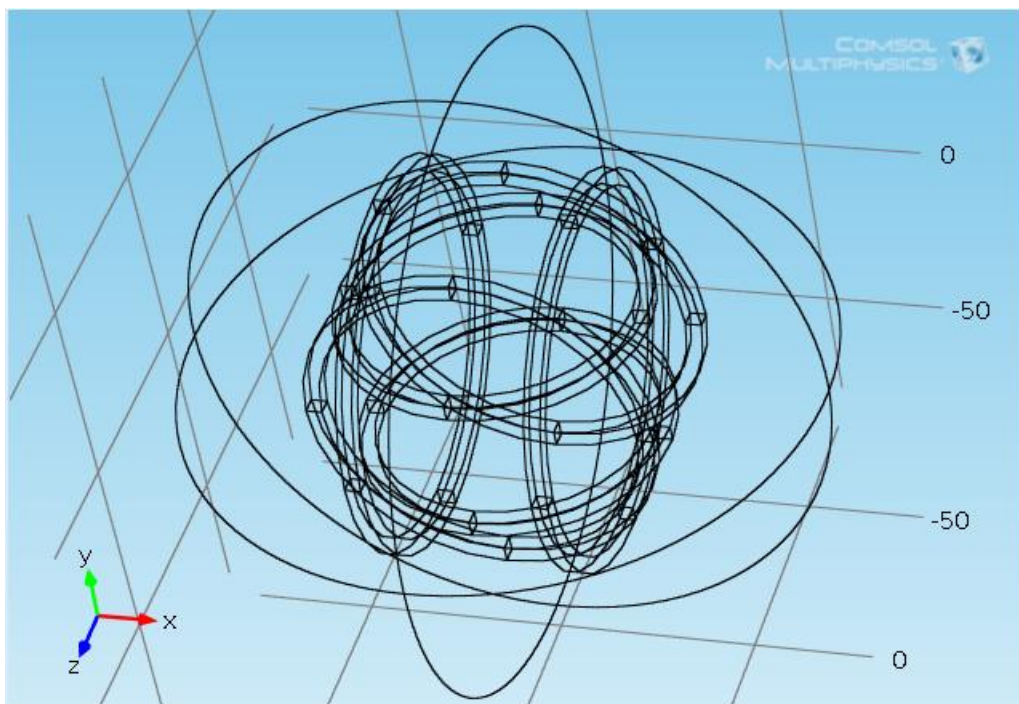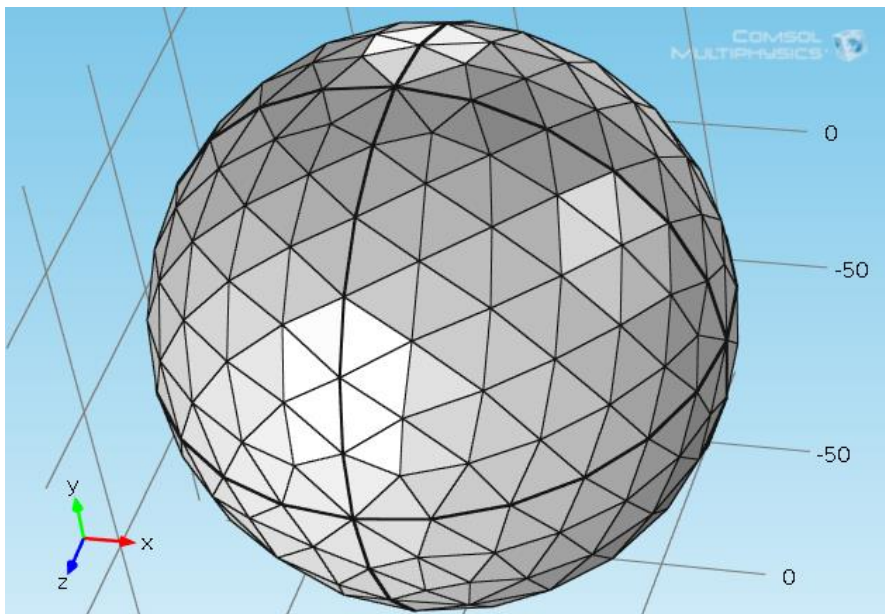

Fig 3.3: The 3D model

The magnetic fields (mf) subsection of the AC/DC module is selected for the simulation. The coil arrangement is modelled using the geometry tools. Three separate work planes are defined for each plane. First the work plane is created for xy plane, then for yz plane and then for zx plane. For each plane, squares representing the cross-section of the coil are placed considering the radius and the distance between the coils. Then the revolve functionality is used to complete the coil by building the square cross-section for a circular path.

To model the surrounding air, the coil arrangement is encased in a big sphere. Then materials are defined for the coil and the air. For air, the value of relative permeability is given

1, relative permittivity is given 1, and various parameters like electrical conductivity, dynamic viscosity, ratio of specific heats, heat capacity at constant pressure, density and thermal conductivity are given by default. The coil material is defined as copper. For copper, an electrical conductivity of $5.998*10^7$ S/m is given, coefficient of thermal expansion is given a value of $17 * 10^{-6}$ 1/K, thermal conductivity is given a value of 400 W/m.K, Young's modulus is given a value of $110*10^9$ Pa and Poisson's ratio of 0.35.

The coils are defined as multi turn coils in the magnetic field section. Each coil is defined in a separate domain .The value of current and the number of turns are entered for each coil pair as given above. Circular coil type is selected for each coils. The constitutive relation for magnetic field is $B = \mu_0\mu_r H$. For specifying the direction of wires in the coil, a Reference edge sub feature is added and a group of edges forming a circle are selected. Then the software automatically computes the path of the wires from the geometry of the selected edges. The entire geometry is divided for computation using mesh command. The element size is chosen coarse and to get finer results free tetrahedral mesh arrangement is applied to the geometry.

The compute command is given and the results are plotted using the 3D plot group in the results subsection. The magnetic flux density and the flux profile in the xy plane is plotted. Magnetic flux density is given in Tesla. The mf.normB expression is used to compute the flux density. The Slice function is used to select the xy plane and the Arrow Volume is used to plot the magnetic field lines. The expression mf.Hx, mf.Hy and mf.Hz are chosen for plotting the field in x, y and z directions.
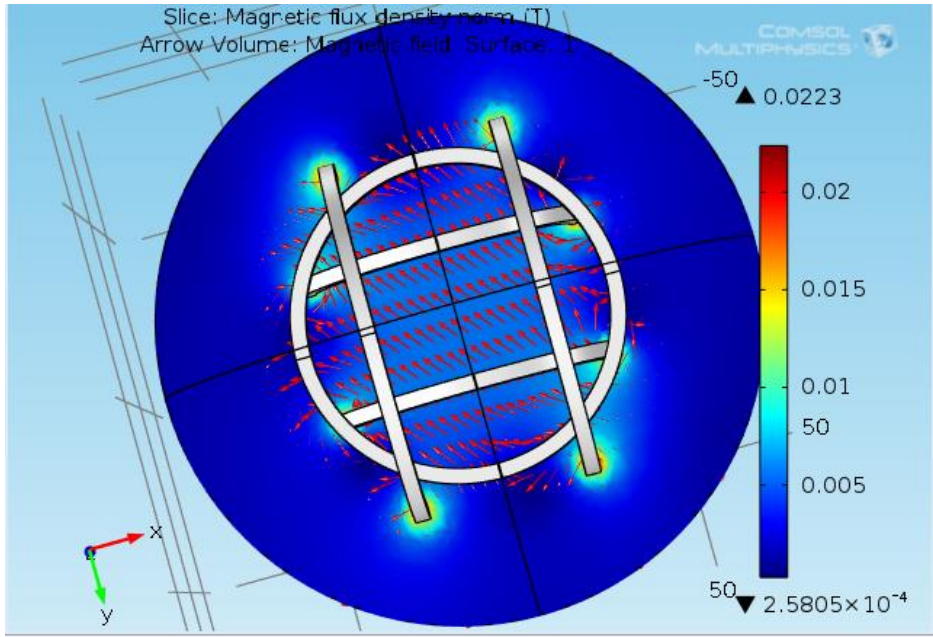
The value of magnetic field at various points are:

SL.NO	X (CM)	Y (CM)	Z (CM)	VALUE (T)
1	4.58588	-7.78668	1.42109e-14	0.00563
2	0.53854	-6.34108	0	0.00562
3	6.87729	6.11603	4.263e-14	0.00566
4	-15.21519	10.94814	2.842e-14	0.00568

3.2.4 Conductive Heat Transfer in the Pumping Cell

The rubidium in the pumping cell is to be maintained in its vapour form. For this purpose the oven is continuously circulated with hot air from a blower. The following simulation is done to build and solve the conductive heat transfer problem between the hot air that is outside and the cold air that is inside, through the Pyrex pumping cell. The heat transfer profile is plotted and studied. The model shows an axisymmetric steady state thermal analysis. The following model domain describes a cross-section of the 3D model. This model was simulated using the Heat transfer in solids subsection of the Heat Transfer module.
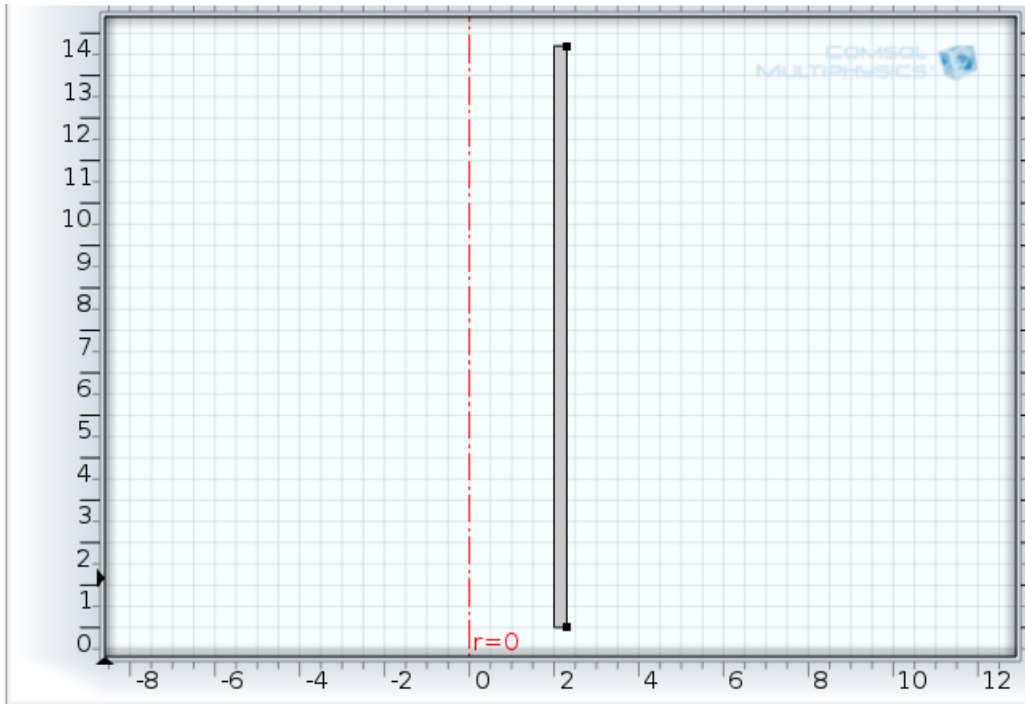
The boundary conditions prescribed are:

1. Prescribed heat flux

2. Initial temperature inside the cell.

The steady state heat equation for conduction with volumetric heat source made zero is the governing equation for this problem [13].

$$\nabla.(-k\nabla T) = 0$$

Where k is the thermal conductivity. The model is first created in 2D axisymmetric mode and then converted to 3D. First a 2D rectangle with length equal to the length of the coil and width equal to the width of the coil is placed at a distance equal to the radius of the cell from the centre. Then the various boundary conditions ae given. The initial temperature inside the cell is 303 K. The heat flux on the cell wall is 77447.66 W/m². The thermal conductivity of the glass is taken as 1.38 W/(m.K). Other properties of the glass given are electrical conductivity of $1*10^{-14}$ S/m, Coefficient of thermal expansion $0.55 * 10^{-6}$ 1/K, heat capacity at constant pressure 703 J/kg.K, relative permittivity of 2.09, density of 2203 kg/m³ and Young's modulus of $73.1 * 10^9$ Pa. The mesh is plotted with normal element size. The mesh consists of 68 elements.
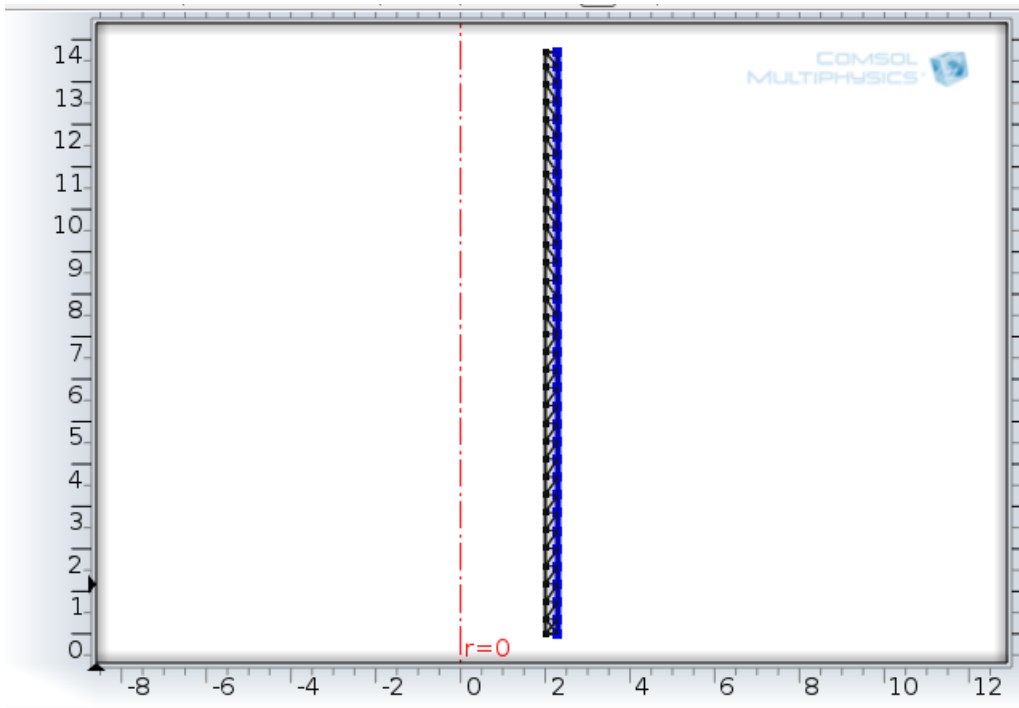
The temperature profile is plotted in 3D. The color range has a minimim value of 250 K and a maximum value of 550 K.
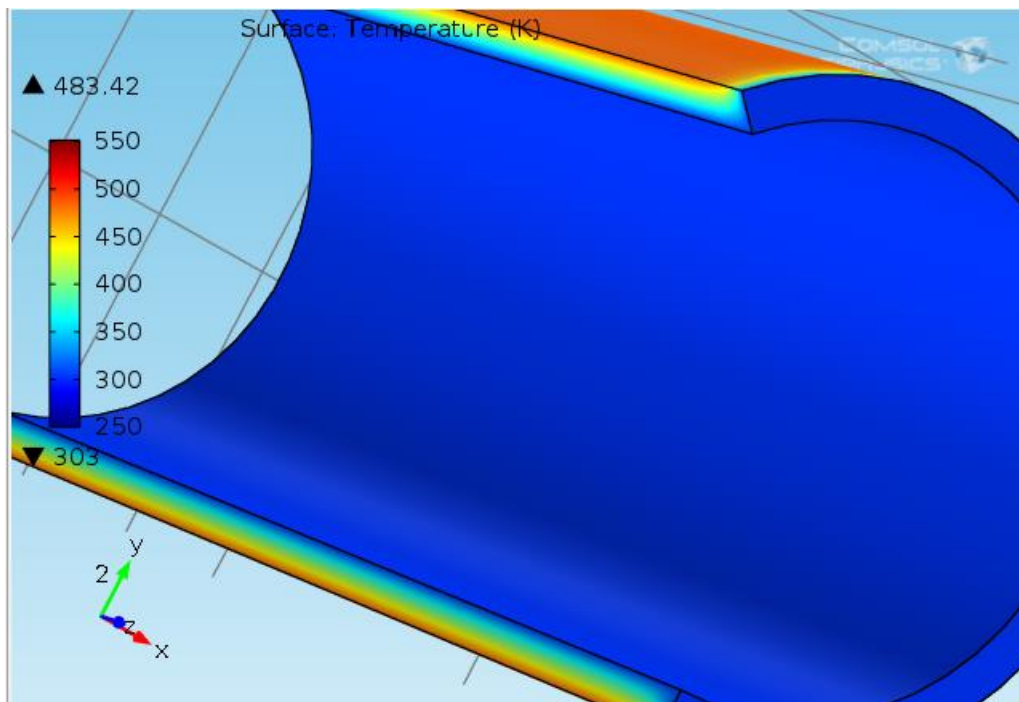
The value of temperature at various points are:

SL.NO	X (CM)	Y (CM)	Z (CM)	VALUE (K)
1	-1.34286	1.8628	11.48827	483.40942
2	-1.56619	1.56619	12.69589	433.70725

3	-1.52372	1.52372	12.84316	397.55028
4	1.32813	1.49407	7.49466	303

3.2.5 Turbulent Flow through Condenser Pipe

After the polarization in rubidium is transferred to xenon, the polarized xenon gas is to be separated. For this the gas mixture is flushed with high pressure nitrogen gas. The gas passes through a helical condenser pipes placed in liquid nitrogen gas. The heat and velocity profile of the gases as it passes through the pipes are plotted here. The figure below shows the diagram of one coil of condenser. It is surrounded by nitrogen gas at a temperature of 77.2 K. The gas mixture in the pipe will be at a temperature of 140 °C. Here we will simulate the flow of air at the same temperature instead of gas mixture. The tube is made of stainless steel.

One of the important characteristic of the flow is the Reynolds number, Re, defined as:

$$Re = \frac{UL}{\eta}$$

Where U is velocity scale, L is length scale and η is kinematic viscosity. If the Reynolds number is high, the flow is dominated by convection and turbulence model is necessary. Since the gas mixture will be flushed from the cell using a high pressure nitrogen gas, the flow here is turbulent. The Fluid Flow module was used to model this. The governing equations in this model are:

1. The Reynolds-averaged Navier Stokes (RANS) equation and a $k - \varepsilon$ turbulence model.

2. The heat transfer equations in air and in steel tube walls.

The non-isothermal flow multiphysics coupling is used in order to model the fluid thermal interaction. The temperature dependent properties for water and steel are used from the built in material library.

The boundary conditions for the problem are:

1. $k - \varepsilon$ equations in the fluid domain:

2. Heat transport equations.

The model is created using various tools in the geometry section. The circle tool is used to fix the two boundaries. Two circle built the inner boundary and two circles built the outer boundary. The difference Boolean operation is used to cancel out the unwanted portion to get the area of interest. Compose Boolean operation is used to make path for the inlet and outlet portions.

The steel defined has a heat capacity at constant pressure of 475 J/kg.K, density of 7850 kg/m^3, thermal conductivity of 44.5 W/(m.K), electrical conductivity of 4.032 * 10^6 S/m, coefficient of thermal expansion of 12.3 * 10^{-6}, Young's modulus of 205 * 10^9 Pa and a Poisson's ratio of 0.28.
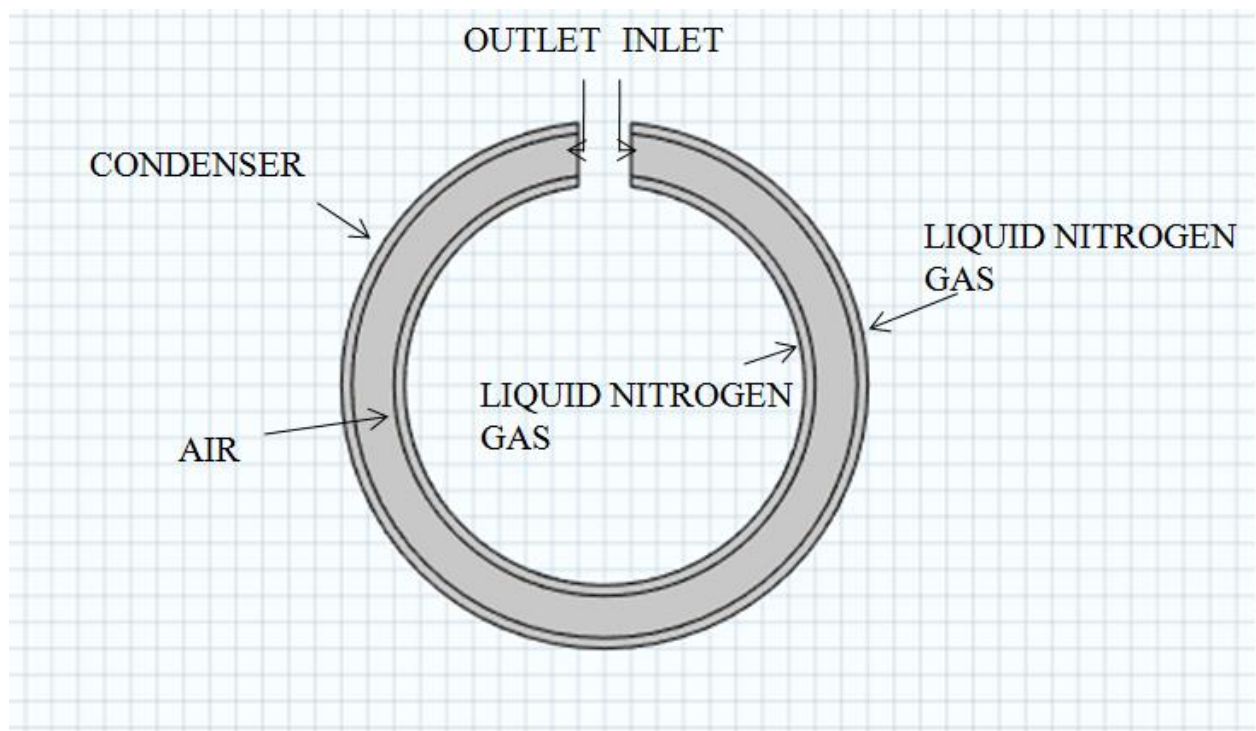
The physics induced sequence is used for mesh generation. The different physics domains are treated differently. For the solid domain the mesh size is fine and for the fluid domain the mesh size is extra fine. The complete mesh consists of 6706 elements.
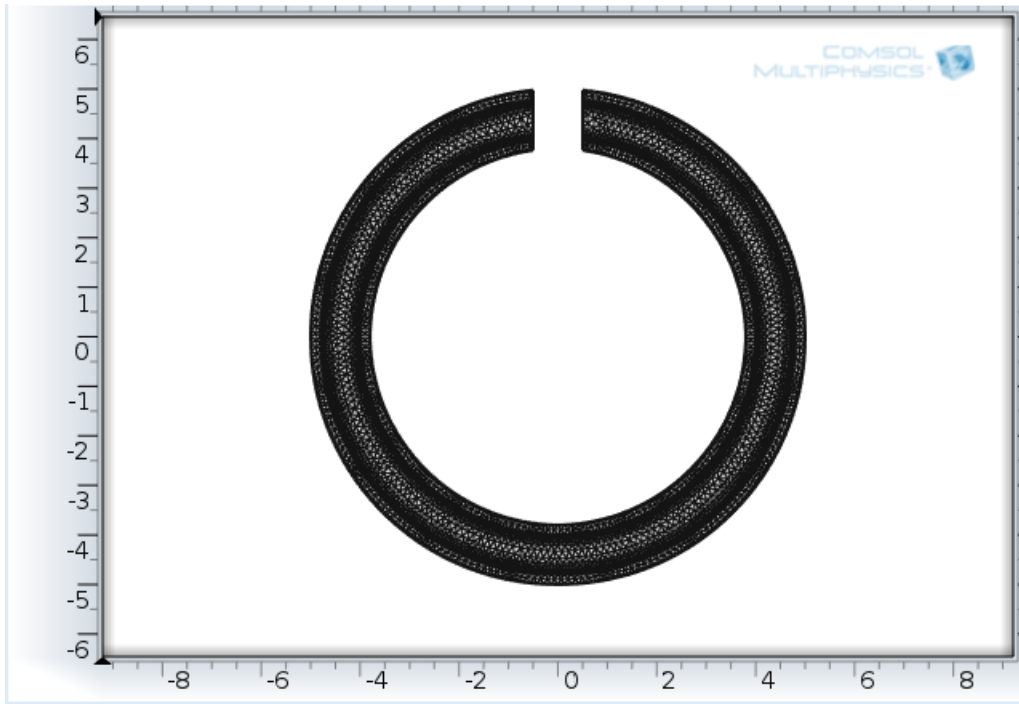
The velocity profile is then plotted in the results section. The nitf.U expression is used to plot the velocity magnitude. The unit is m/s. The colour range has a minimum value of 0.00214 m/s and a maximum value of 5.5 m/s.

Surface: Velocity magnitude (m/s)
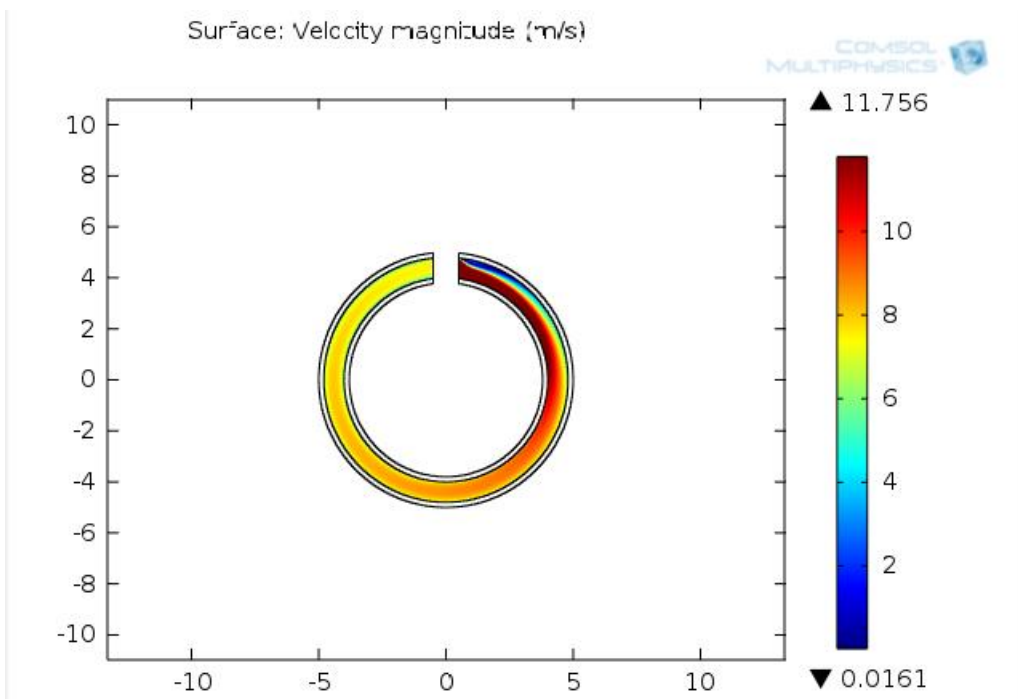
The velocity magnitude at various points are:

SL.NO	X (CM)	Y (CM)	VALUE (m/s)
1	0.6749	4.46302	6.26974
2	1.54573	4.46302	0.56018
3	2.37302	3.63573	5.77402
4	4.3324	1.7199	2.96348

For the temperature profile, the colour range has a minimum value of 77.2 K and a maximum value of 600 K.

Surface: Temperature (K)
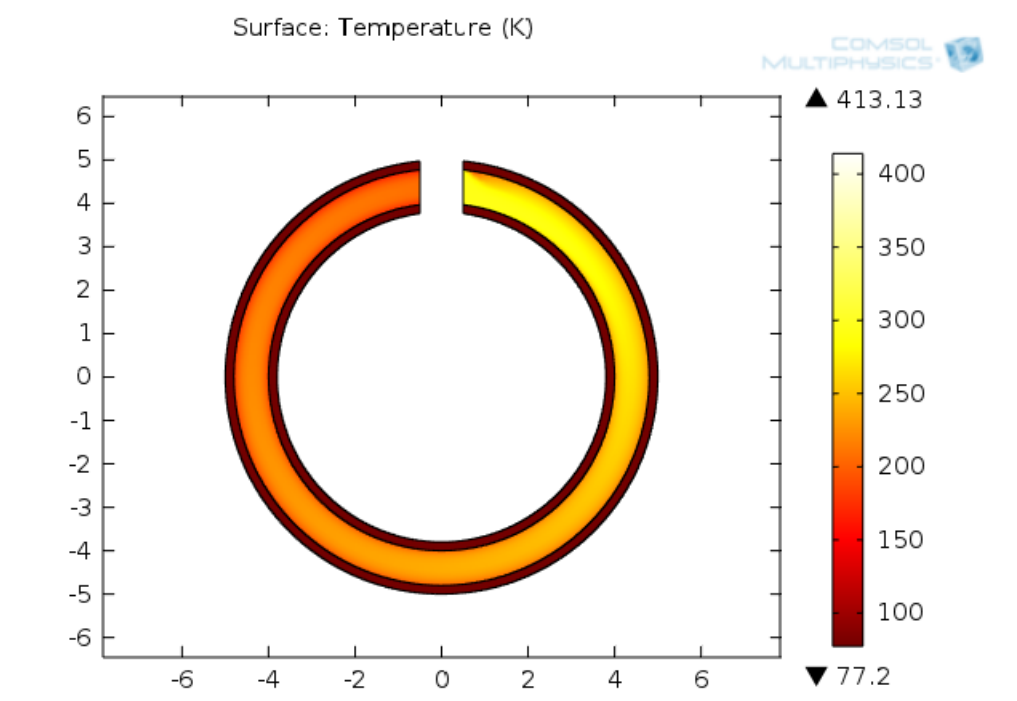
The temperature magnitude at various points are:

SL.NO	X (CM)	Y (CM)	VALUE (K)
1	0.71844	4.3324	412.01164
2	1.28448	4.20177	402.79735
3	3.67927	2.32948	394.75235
4	-3.94052	-1.9376	309.4986

3.2.6 Modelling the Magnet System used in Polarizer

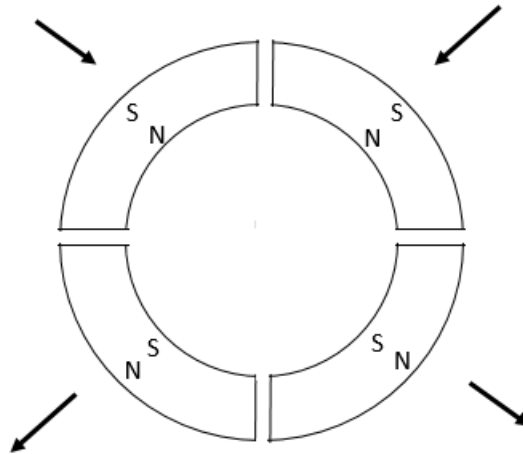Here we will be modelling the following magnet design:


Fig 3.4: magnetization directions

This arrangement of magnet is used in our lab to preserve the hyperpolarization in xenon. The domain consists of five regions:

1. Four arcs of the magnet

2. The air surrounding the magnet

The permeability of air is $\mu = 4\pi \times 10^{-7}$. The relative permeability of the magnet pieces are 2,00,000. The pre-magnetization in the magnets is shown as arrows in the above figure. The net magnitude of pre-magnetization is 750000 A/m. The magnet is modelled using magnetostatics subsection in the electromagnetics module. The tools in the geometry section are used to model the magnet arrangement. The arcs are constructed using the Bezier polygon tool and are defined as open curve. The arcs are created minding the gap between each magnet piece and also the width of the magnet. The ends of each arc are joined by line tool. The magnetization conditions are given as mentioned above. The normal size is chosen for the mesh. The mesh consists of 2360 elements. For the air domain the default constitutive relationship $B = \mu_0\mu_r H$ is used and for the magnet domains, the constitutive relationship $B = \mu_0 H + \mu_0 M$ is used.
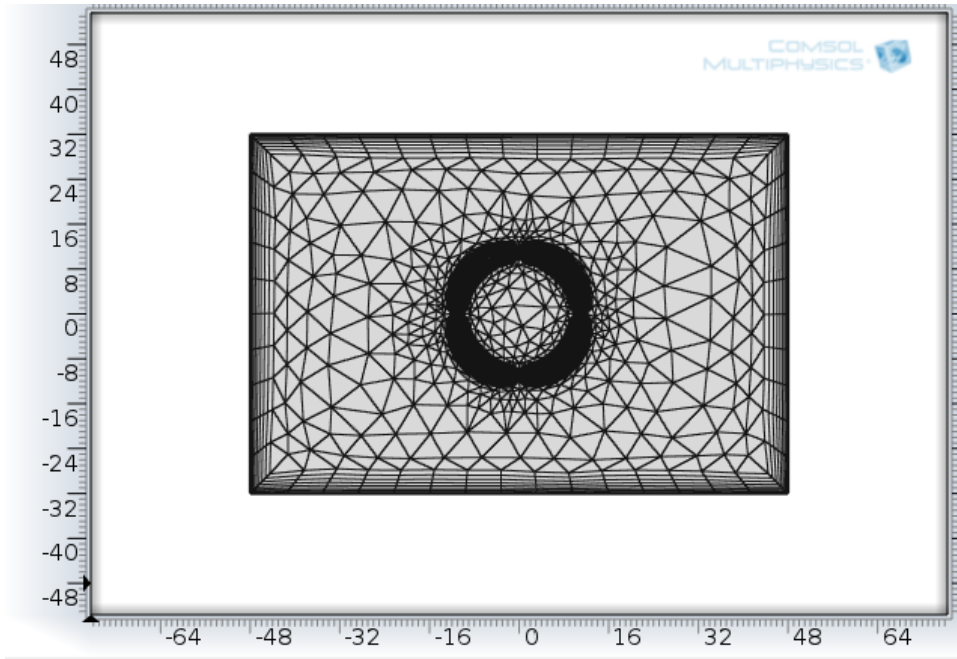
Then the model parameters are computed. The magnetic flux density 2D plot gives the values of flux density in T. The expression used is mfnc.normB. The output display colour range has a minimum value of 4.2011e-6 T and a maximum value of 0.6 T.

Surface: Magnetic flux density norm (T)
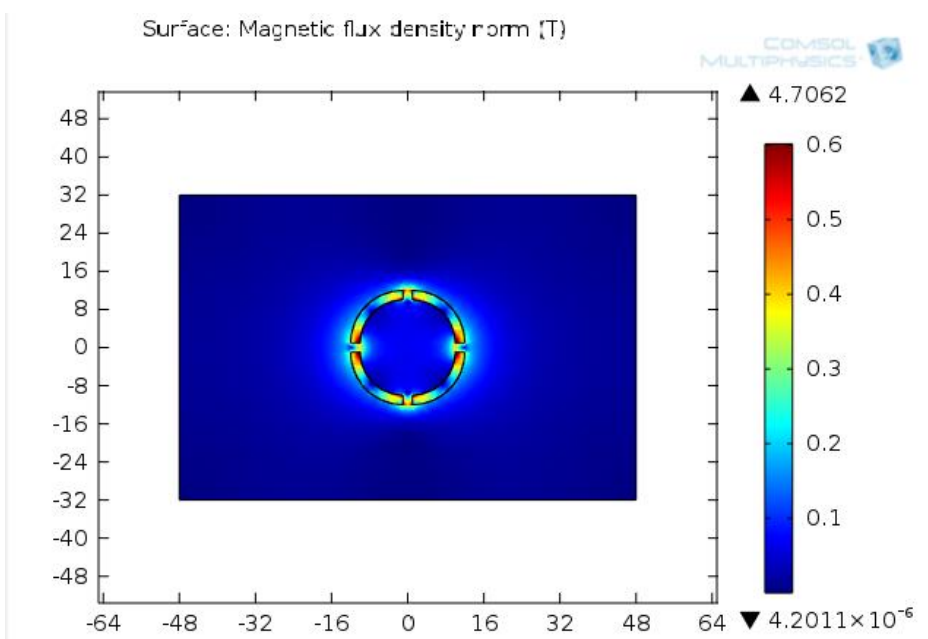
The magnetic flux density values at various points are:

SL.NO	X (CM)	Y (CM)	VALUE (T)
1	0.15363	-0.76815	0.06764
2	9.98598	3.84076	0.3935
3	-0.46089	0.46089	0.06765
4	-6.29885	-4.14802	0.05736

The streamline plot is used to visualize the magnetic field by using field lines. The distance between the lines and the magnetic fields are inversely proportional. The expression used for x component is mfnc.Bx and for y component it is mfnc.By.
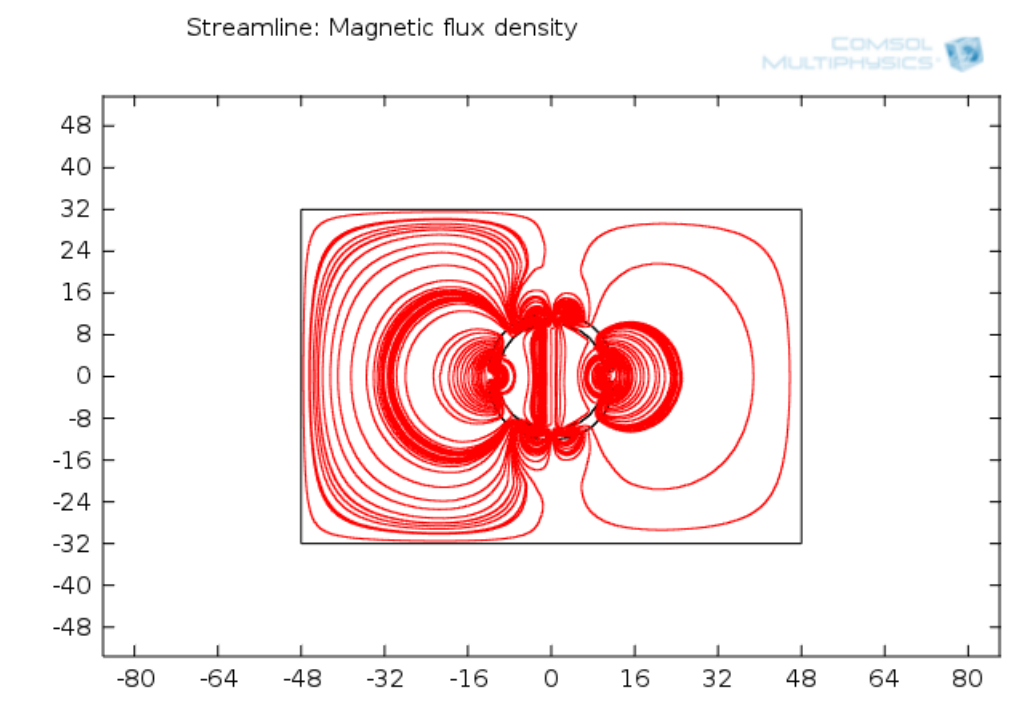
3.2.7 Modelling a Linear Halbach Array

A linear Halbach array as shown in the figure below is to be modelled. This arrangement provides a strong magnetic field for the preservation of the hyperpolarization in xenon.
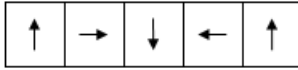
Fig 3.5: magnetization directions

The domain consists of 6 regions:

1. 5 blocks of magnet.

2. The air surrounding it.

The permeability of air is $\mu = 4\pi \times 10^{-7}$. The relative permeability of the magnet pieces are 200,000. The pre-magnetization in the magnets is shown as arrows in the above figure. The net magnitude of pre-magnetization is 750000 A/m. The magnet is modelled using magnetostatics subsection in the electromagnetics module. The tools in the geometry section are used to model the magnet arrangement. The rectangle tool is used to build the individual magnet pieces. The object type is chosen as curve for each rectangle. The surrounding air is modelled by placing a larger rectangle over the magnets. The magnetization conditions are given with the magnitude and directions as mentioned above. The normal size is chosen for the mesh. The mesh consists of a total of 1198 elements. For the air domain the default constitutive relationship $B = \mu_0 \mu_r H$ is used and for the magnet domains, the constitutive relationship $B = \mu_0 H + \mu_0 M$ is used.
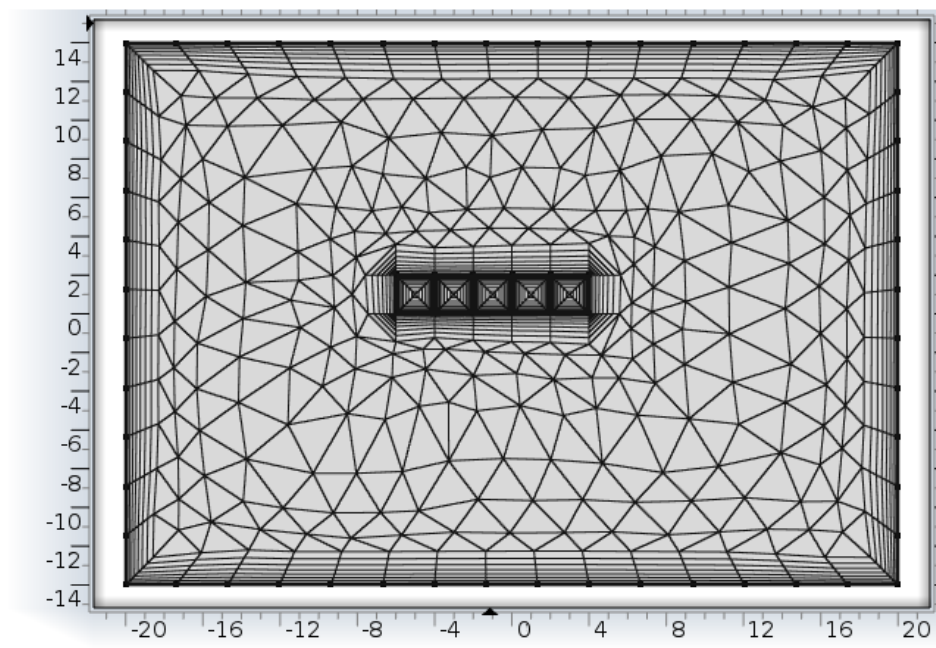
Then the model parameters are computed. The magnetic flux density 2D plot gives the flux density values. The expression used for plotting is mfnc.normB. The colour range has a minimum value of 5.689e-7 T and a maximum value of 1.11724 T.

Surface: Magnetic flux density norm (T)
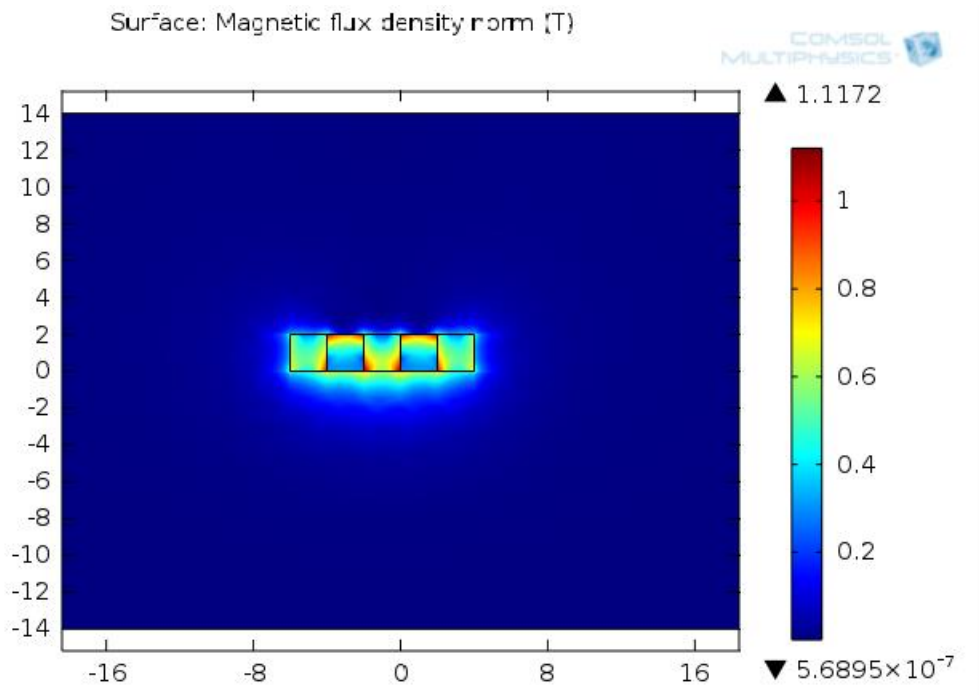
The values of magnetic flux density at various points are:

SL.NO	X (CM)	Y (CM)	VALUE (T)
1	-4.55607	1.07503	0.55014
2	-2.81555	1.38218	0.54411
3	-1.27979	1.07503	0.5397
4	-0.87026	-0.87026	0.36165

The streamline plot is used to visualize the magnetic field by using field lines. The distance between the lines and the magnetic fields are inversely proportional. The expression for x component is mfnc.Bx and the expression for y component is mfnc.By.

Streamline: Magnetic flux density

COMSOL MULTIPHYSICS
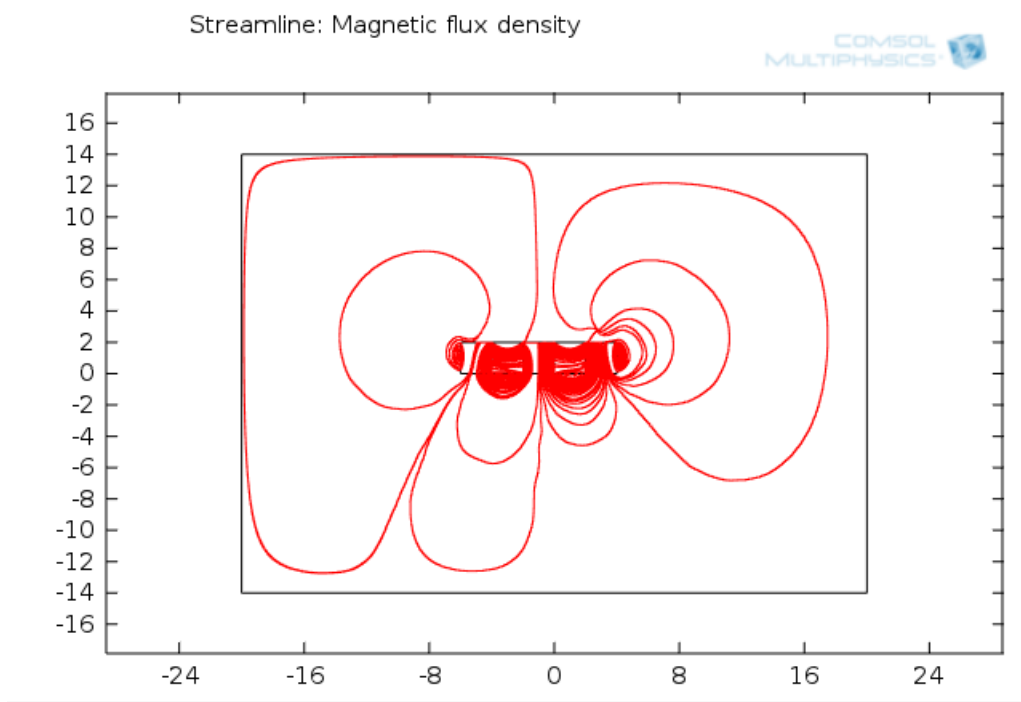
3.2.8 Modelling a Halbach Cylinder

The following magnet design is modelled:

Fig 3.6: magnetization directions

This arrangement provides a really uniform and strong magnetic field inside the cylinder. The domain consists of 10 regions:
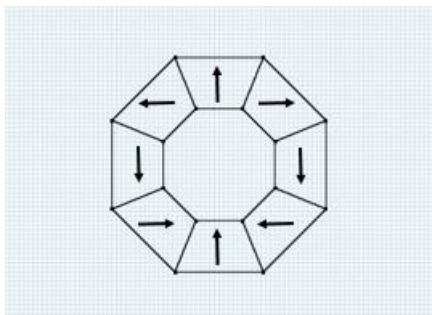
1. 8 blocks of magnet.

2. The air surrounding it.

3. The air inside the cylinder.

The permeability of air is $\mu = 4\pi \times 10^{-7}$. The relative permeability of the magnet pieces are 2,00,000. The pre-magnetization in the magnets is shown as arrows in the above figure. The net magnitude of pre-magnetization is 750000 A/m. The magnet is modelled using the tools in the geometry section. Bezier polygon is to model the outer and inner boundary of the cylinder. The maget separations are modelled using the line tool. All the sections are defined as type open curve. The outer air boundary is defined by placing the large rectangle. The extremely fine size is selected for the mesh. The mesh consists of a total of 46280 elements. For the air domain the default constitutive relationship $B = \mu_0 \mu_r H$ is used and for the magnet domains, the constitutive relationship $B = \mu_0 H + \mu_0 M$ is used.
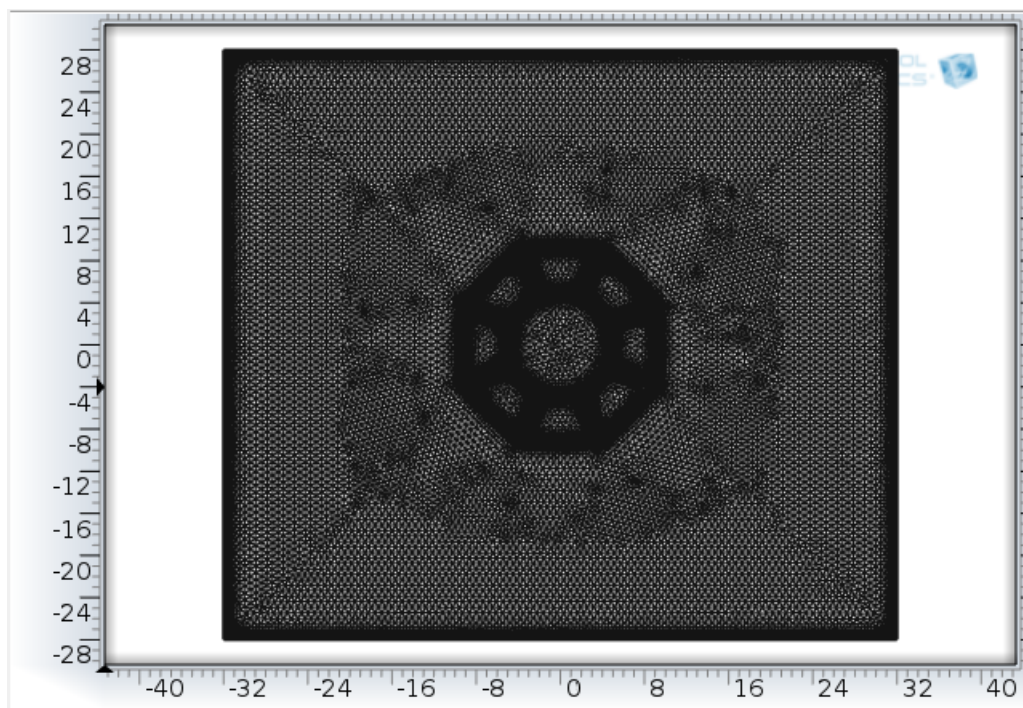
Then the model parameters are computed. The magnetic flux density 2D plot gives the flux density values. The expression used is mfnc.normB. The colour range has a minimum value of 4.2074e-10 T and a maximum value of 1.2 T.

Surface: Magnetic flux density norm (T)
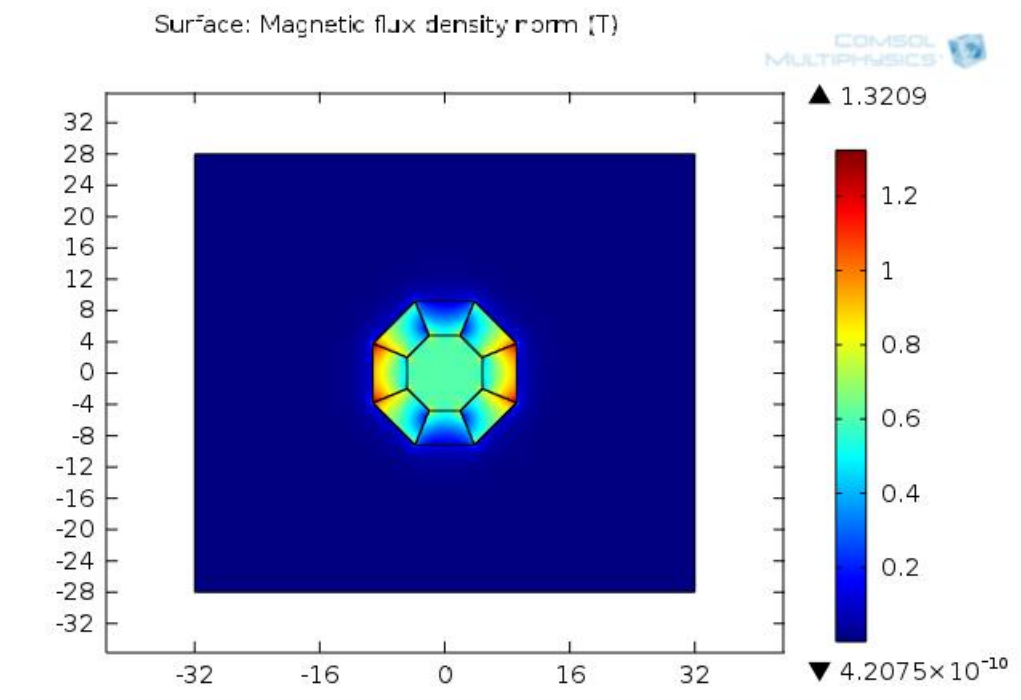
The value of magnetic field at various points are:

SL.NO	X (CM)	Y (CM)	VALUE (T)
1	-1.13123	-1.65333	0.55096
2	7.91858	2.85157	0.87289
3	-0.43509	-0.60912	0.55096
4	-2.0014	-2.0014	0.55025

The streamline plot is used to visualize the magnetic field by using field lines. The distance between the lines and the magnetic fields are inversely proportional. The expression for x component is mfnc.Bx and the expression for y component is mfnc.By.

Streamline: Magnetic flux density
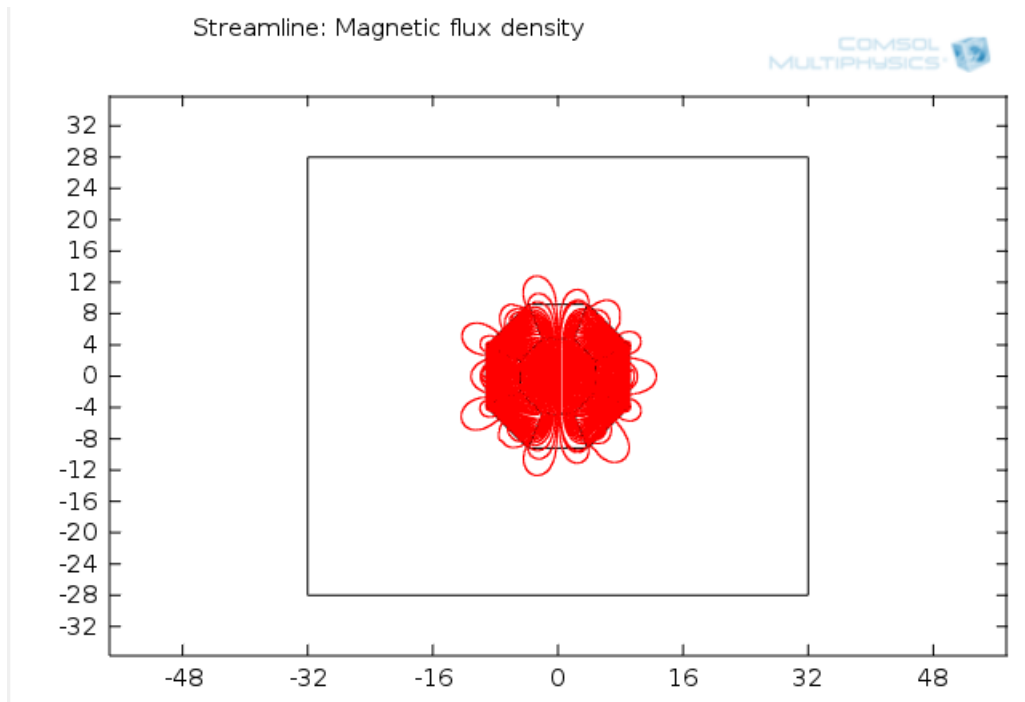
3.2.9 Modelling a Magnet Arrangement Using Four Dipoles

The following magnet system is modelled here:
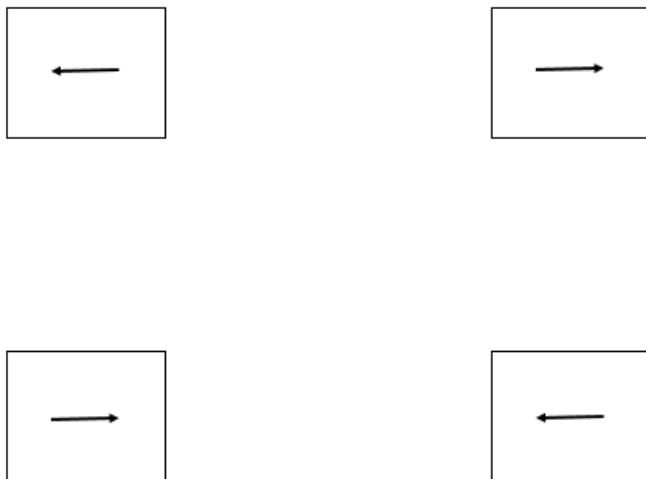
Fig 3.7: magnetization directions

The arrangement provides a strong and uniform magnetic field inside the magnet. The entire model consists of 6 domains:

1. The four magnets

2. The air surrounding the magnets.

The permeability of air is $\mu = 4\pi \times 10^{-7}$. The relative permeability of the magnet pieces are 2,00,000. The pre-magnetization in the magnets is shown as arrows in the above figure. The net magnitude of pre-magnetization is 750000 A/m. The rectangle tool is used to place the four magnets. The air domain is modelled by placing a larger rectangle. The extra fine size is selected for the mesh. The mesh has a total of 8318 elements. For the air domain the default constitutive relationship $B = \mu_0\mu_r H$ is used and for the magnet domains, the constitutive relationship $B = \mu_0 H + \mu_0 M$ is used.
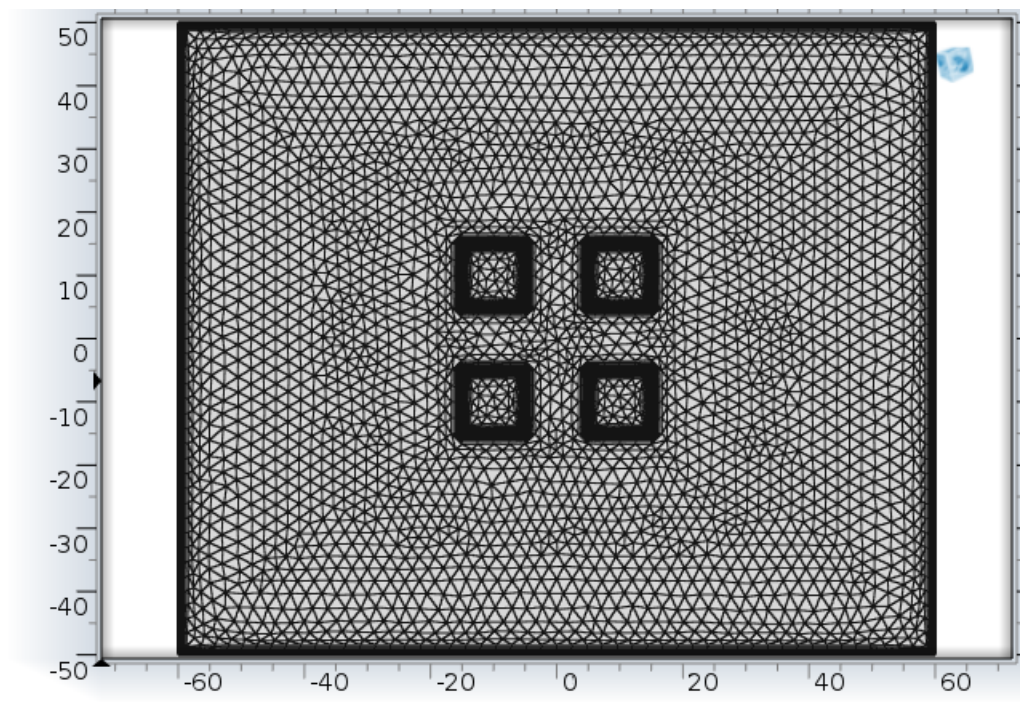

Then the model parameters are computed. The magnetic flux density 2D plot gives the flux density values. The expression used is mfnc.normB. The colour range has a minimum value of 1.095e-6 T and a maximum value of 0.8686 T.

Surface: Magnetic flux density norm (T)
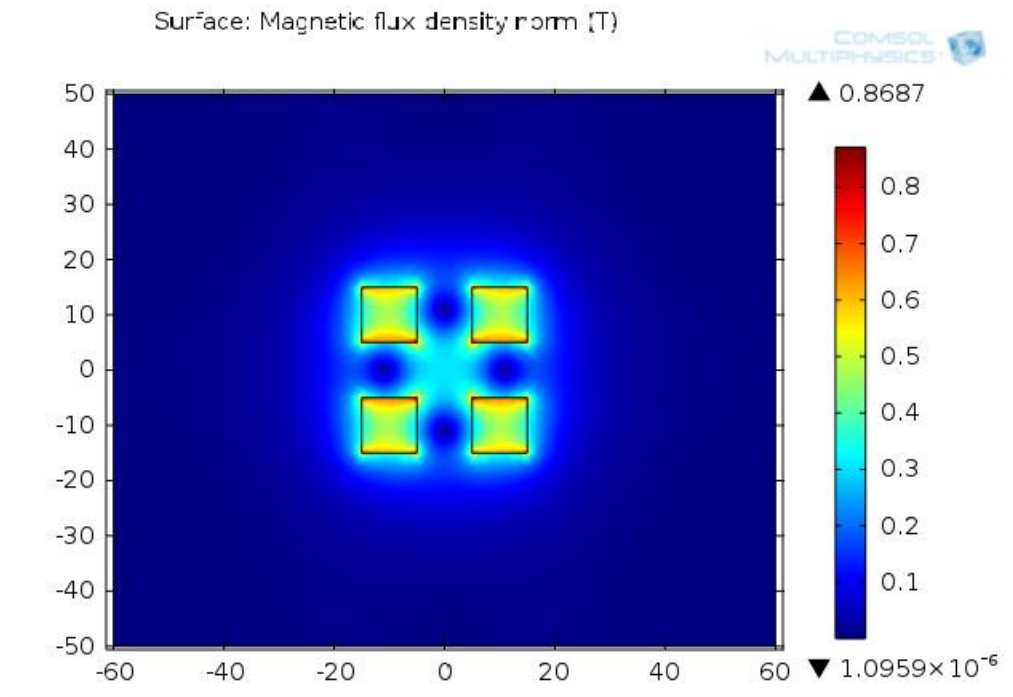
The magnetic flux density values at various points are:

SL.NO	X (CM)	Y (CM)	VALUE
1	0.17064	1.19448	0.3066
2	0.51192	7.67877	0.17297
3	8.36133	10.06772	0.447
4	3.58343	-2.55959	0.32925

The streamline plot is used to visualize the magnetic field by using field lines. The distance between the lines and the magnetic fields are inversely proportional. The expression for x component is mfnc.Bx and the expression for y component is mfnc.By.

Streamline: Magnetic flux density
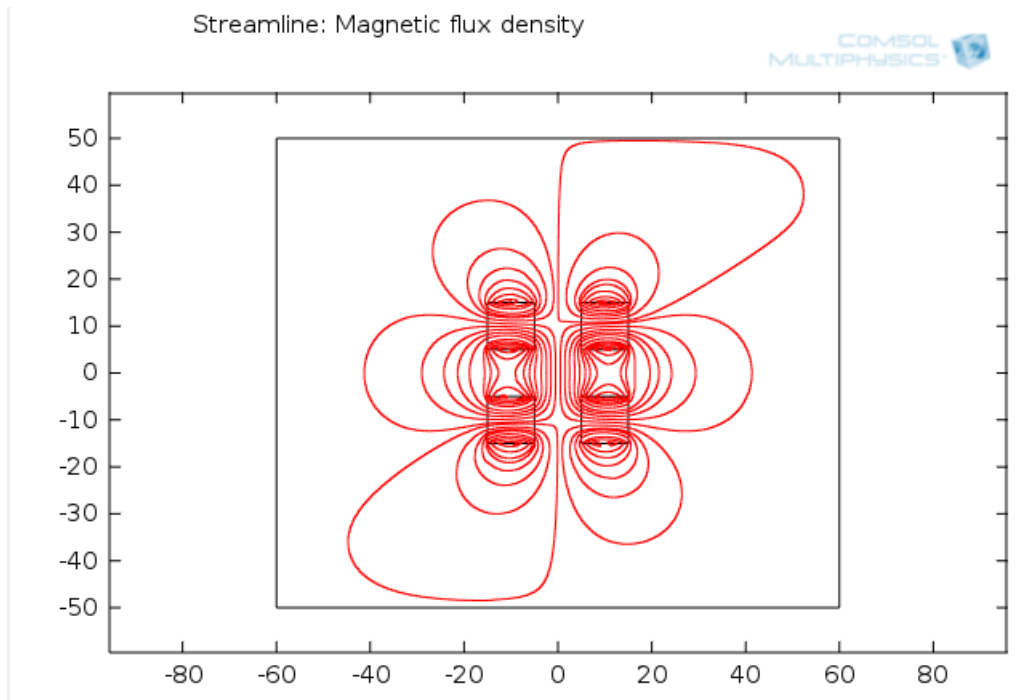
3.3 Testing of a Few Polarizer Components

3.3.1 Procedure for the Starting and Shutting Down of the Laser System

3.3.1.1 Start-up Procedure of Laser

1. Switch on the chiller, pump and cool, then set water temperature to 18 C and wait about 10 minutes until the temperature has stabilized.
2. Switch on electronics control box to turn ON the TECs.
3. Click on the SHARK LS software and make sure that all two TECs are communicated by looking at real time temperature does not read the actual temperature, the communication connection is not properly established.
4. Click Ext Log for recording the operating parameters for understanding the system performance.
5. On the SHARK LS software screen, click the ON button to turn the TEC temperature control for the laser diode and the VBG ON. The ON power status of the box must be green. If LD power and VBG power do not respond, the TEC power supply may not be properly installed.
6. Turn the front panel AC switch of the laser diode power supply to ON.
7. Slowly increase the current to the laser diode to 48A and voltage should be around 4V.

8. Observe the laser diode temperature in the software to make it cool down to the set point and does not exceed 40 C at any time

9. Observe laser output.

3.3.1.2 Shutdown Procedure of Laser

1. Turn the current to the laser diode down to 0A.

2. Using the software turn the TEC temperature controllers power off. Wait until the zero number in the LD and VGB power turn black colour and then turn OFF software.

3. Turn switch of TEC controllers OFF.

4. Wait 10 minutes before shutting the chiller OFF.

3.3.2 Testing the Polarity of Light

3.3.2.1 Description

For optical pumping to take place, the light entering the cell must be circularly polarized. The light from the laser is unpolarised light. To make it circularly polarized first it has to be made linearly polarized. The unpolarised light is made linearly polarized by passing it through a polarizing beam splitter (PBS) cube and later is made circularly polarized by passing it through the quarter wave plate. A 5 mW laser is used for the testing purpose.

3.3.2.2 Aim

To test the polarity of the light after it passes through the PBS cube and through the quarter wave plate.
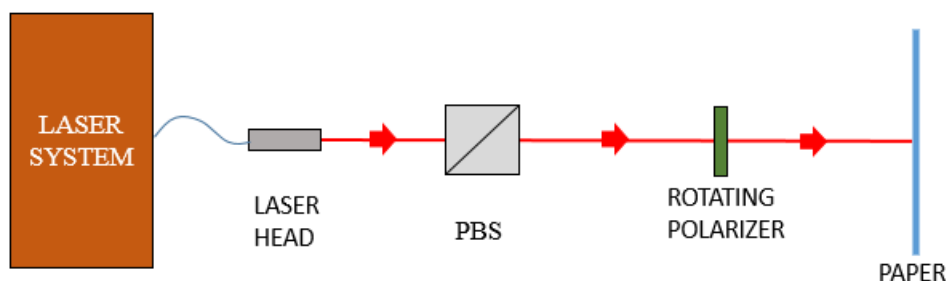
3.3.2.3 Diagrams

Fig 3.8: arrangement for detecting the polarity of light after passing through PBS
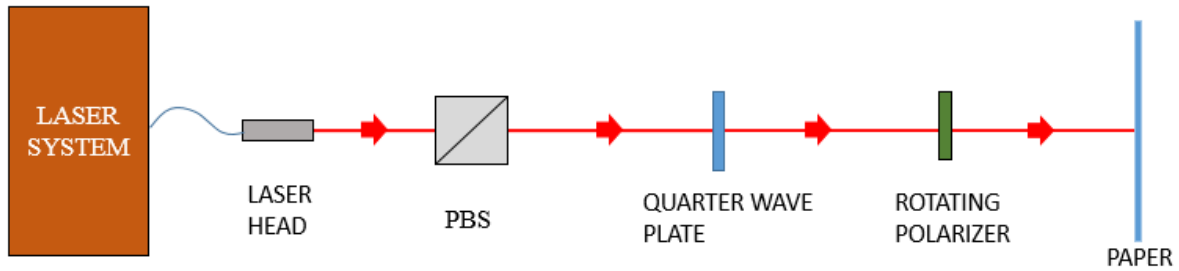
Fig 3.9: arrangement for detecting the polarity of light after passing through quarter wave plate

3.3.2.4 Procedure

1. Testing the polarity of light after passing through the PBS cube

First the arrangement is made as in Fig. 3.8 and the light intensity is observed on the paper. The rotating polarizer is rotated 360 degrees and the change in the intensity of light is observed.

2. Testing the polarity of the light after passing through the quarter wave plate.

The components are arranged as in Fig 3.9. The white markings indicating the fast axis is identified. First the quarter wave plate is rotated through +45° (at 0°) and then the light intensity on the paper is observed as the polarizer is rotated. Then the quarter wave plate is rotated through – 45° from the fast axis (at 90°) and the light intensity is observed on the paper as the polarizer is rotated.

3.3.2.5 Observations

The light coming from the PBS cube had a maximum value of intensity when the polarizer was at 90° and had a minimum value at 0°.

For both the cases of quarter wave plate, when the wave plate was at +45° and at -45°, the light intensity on the paper remained unchanged as the polarizer was rotated.

3.3.2.6 Conclusion

As the intensity of the light coming from the PBS cube had a maximum at 90° and a minimum at 0°, this shows that the light was linearly polarized in the vertical direction.

As the intensity of the light coming from the quarter wave plate was not changing in both the cases, this proves that the light is circularly polarized.

3.3.3 Testing the Magnetic Field within the Helmholtz Coil

3.3.3.1 Description

A Helmholtz coil consists of two parallel similar coils wounded in series. The current is in same direction in each coil. The distance between the coils is one radius. The intensity of the magnetic field produced is directly proportional to the number of turns and the current through the coil. Within the coil, the field component parallel to the axis gets added and the vertical component gets cancelled. This creates a uniform magnetic field between the coils. The Helmholtz coil provides the necessary uniform magnetic field to the pumping cell. The pumping cell is placed as shown in the figure below. The coil radius is 36.6 cm and the number of turns is 334. A 0-50 V/ 8 A DC regulator is used to regulate the power supply to the Helmholtz coil. The magnetic field strength at the points on the pumping cell is measured using a gauss meter. The same is also simulated using COMSOL.

3.3.3.2 Aim

To test the intensity of the magnetic field within the Helmholtz coil arrangement and the results are compared with the simulation results obtained.

3.3.3.3 Diagram
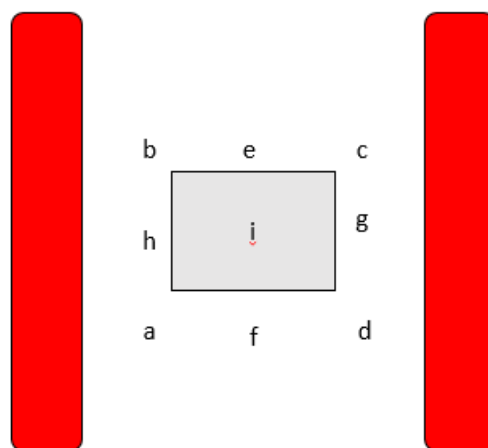
Fig 3.10: top view of the arrangement

3.3.3.4 Procedure

The power supply to the Helmholtz coil is switched on. Then the readings at the corners of the pumping cell as shown in the diagram is taken. The current and the voltage reading from the DC voltage regulator are also noted.

3.3.3.5 Readings

Table 3.1: magnetic field strength within Helmholtz coil

TIME	I (A)	V (V)	a	b	c	d	e	f	g	h	i
0	5.78	51.5	37	37	37	37	37	37	37	37	37
5	5.66	51.5	36	36	36	36	36	36	36	36	36
10	5.55	51.7	36	36	36	36	36	36	36	36	36
15	5.48	52.0	35	35	35	35	35	35	35	35	35
20	5.38	51.6	35	35	35	35	35	35	35	35	35
25	5.37	51.8	35	35	35	35	35	35	35	35	35
30	5.35	51.9	35	35	35	35	35	35	35	35	35
35	5.33	52.0	34	34	34	34	34	34	34	34	34
40	5.28	51.8	34	34	34	34	34	34	34	34	34
45	5.25	51.9	34	34	34	34	34	34	34	34	34
50	5.20	51.6	34	34	34	34	34	34	34	34	34
55	5.21	51.7	34	34	34	34	34	34	34	34	34
60	5.22	52.0	34	34	34	34	34	34	34	34	34
65	5.23	52.2	34	34	34	34	34	34	34	34	34

3.3.3.6 COMSOL Simulation
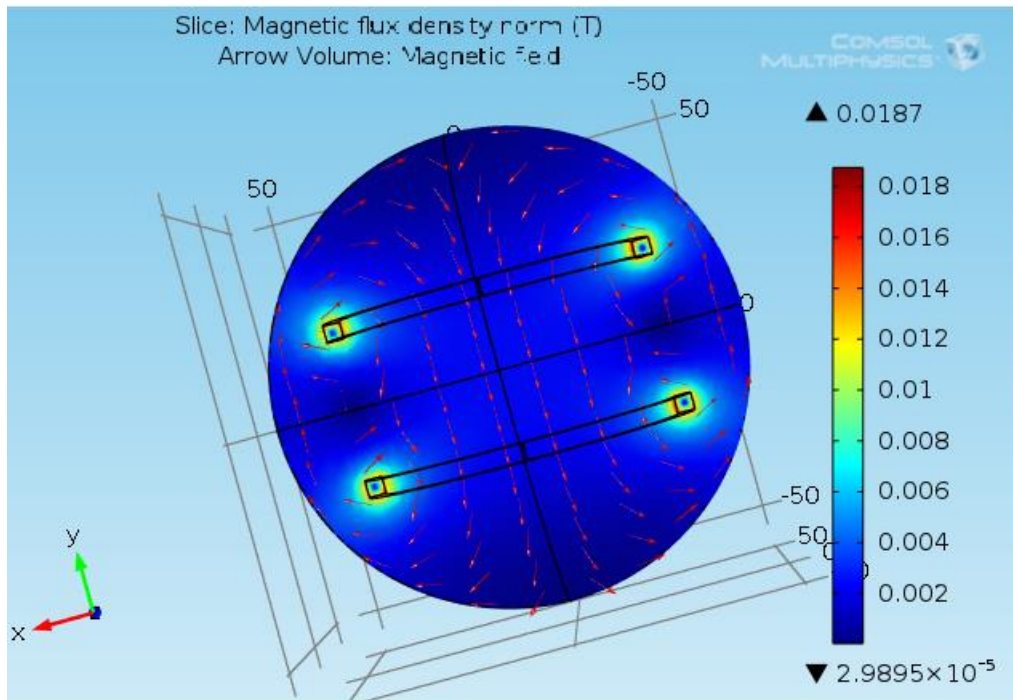
3.3.3.7 Conclusion

The magnetic field strength between the coils was initially 37 G and it kept on decreasing till it reached 34 G after 35 minutes and it maintained that strength for another 30 minutes. The simulation results also gave uniform magnetic field with sufficient strength to aid in optical pumping process.

3.3.4 Testing the Temperature in the Oven

3.3.4.1 Description

The temperature inside the oven should be around 80 to 160°C to maintain the rubidium vapour density. Sufficient value of vapour density should be maintained, for the optical pumping to take place efficiently. A hot air blower is used to heat the oven and the temperature inside the oven is controlled using a PID controller.

3.3.4.2 Aim

Observing the temperature attained inside the oven and the time required to attain it.

3.3.4.3 Procedure

The power supply to the hot air blower and the temperature controller are switched on and the value of temperature is noted. The set value is 120℃.

3.3.4.4 Readings

Table 3.2: temperature inside oven

TIME (MINS)	TEMP (℃)
0	31.9
5	49.3
10	60.0
15	70.9
20	78.7
25	84.9
30	90.6
35	95.5
40	98.9
45	102.6
50	105.7
55	108.0
60	110.4
65	112.3
70	114.1
75	115.5
80	116.8
85	117.9
90	119.0
95	119.8
100	120.8
105	119.5

110	120
115	120.2

3.3.4.5 Conclusion

The temperature inside the oven attained a value of 120.8°C in 100 mins. This temperature would be sufficient to maintain the rubidium vapour density for optical pumping to take place efficiently.

3.3.5 Magnet Arrangement for Xenon Accumulation

3.3.5.1 Description

A cylindrical magnet arrangement as shown in the figure below is modelled and analysed. This arrangement is used to preserve the polarization in xenon. The xenon coming out from the pumping cell is forced into a phantom using nitrogen gas and is solidified in the phantom using liquid nitrogen. The phantom is kept in the magnet arrangement. At temperatures of 77 K and a magnetic field of ~ 500 G the hyperpolarization of xenon is maintained. The arrangement consists of a total of four arcs. Each arc is made of 6 bar magnets. The magnets are pre-magnetized as shown in the figure. The net magnetization has a value of 750000 A/m.

3.3.5.2 Aim

To test the uniformity and the strength of the magnetic field inside the magnet arrangement for xenon accumulation, to plot the magnetic field profile and comparing it with simulation results.
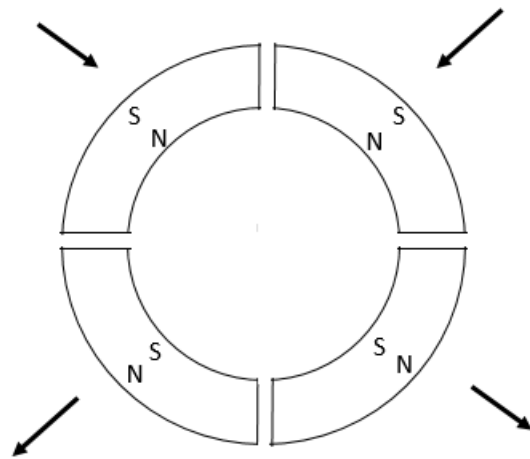
3.3.5.3 Diagrams

Fig 3.11: Magnetization directions
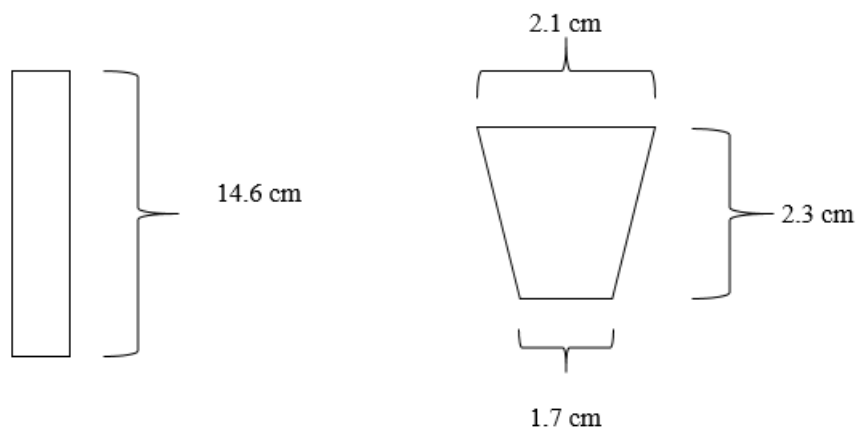
Fig 3.12: Dimensions of bar magnet

3.3.5.4 Model

For getting a net magnetization of 750000 A/m in the resultant direction, a magnetization of 530330.085 A/m is given as its components. To model the surrounding air an air box is placed over the magnet arrangement. Overall the entire model is divided in 5 domains.

1. 4 magnet arcs

2. The air surrounding the magnet.

Magnetization values:

1. M_x = -530330.085 A/m

   M_y = -530330.085 A/m

2. M_x = 530330.085 A/m

   M_y = -530330.085 A/m

3. M_x = -530330.085 A/m

   M_y = -530330.085 A/m

4. M_x = 530330.085 A/m

   M_y = -530330.085 A/m

3.3.5.5 Experimental Results

Table 3.3: magnetic field strength inside the magnet arrangement

BAR NO	TOP	MIDDLE	BOTTOM
1	944	543	582
2	918	838	878
3	864	799	979
4	869	661	1168
5	809	834	1050

6	513	328	38
7	447	137	-540
8	868	749	950
9	869	759	1049
10	952	718	1143
11	1087	969	970
12	348	-770	-882
13	-930	-1010	-1070
14	-940	-774	-961
15	-884	-773	-949
16	-751	-652	-780
17	-750	-633	-863
18	-57	-372	-594
19	-658	-323	-632
20	-563	-309	-692
21	-722	-608	-858
22	-808	-709	-813
23	-462	-597	-719
24	-1250	-828	-931

CENTER

SL. NO	TOP	MIDDLE	BOTTOM
1	349	544	342
2	328	488	342
3	354	560	338
4	444	538	322
5	411	558	353

Magnetic strength around condenser:

AT 10 CM:

SL. NO	A	B	C	D
1	469	448	453	471
2	482	474	407	330
3	453	448	420	408
4	458	449	418	417
5	459	450	429	419

AT 20 CM:

1	528	498	439	438
2	524	508	529	474
3	528	540	454	453
4	533	548	438	508
5	542	505	458	510

AT 30 CM:

1	522	550	524	509
2	529	503	507	472
3	507	506	536	492
4	528	513	492	519
5	509	514	473	504

AT 40 CM:

1	446	462	413	412
2	421	419	423	410
3	447	422	414	420

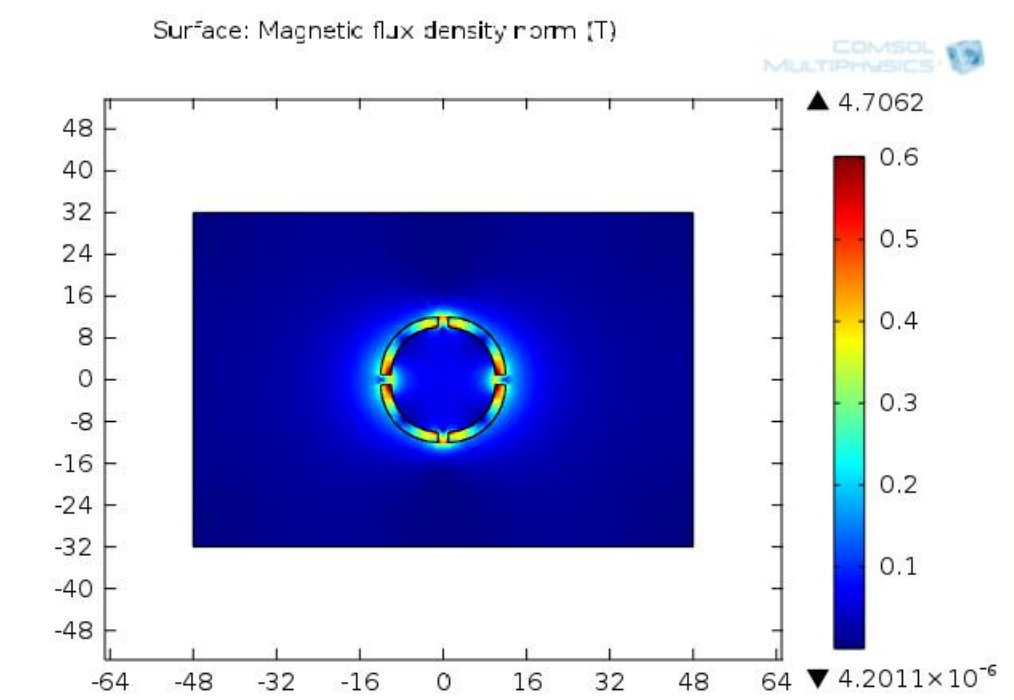| 4 | 472 | 441 | 421 | 403 |
| 5 | 453 | 465 | 468 | 418 |

3.3.5.5.1 Magnet Flux Profile

The magnetic field lines was studied using a magnetic compass.
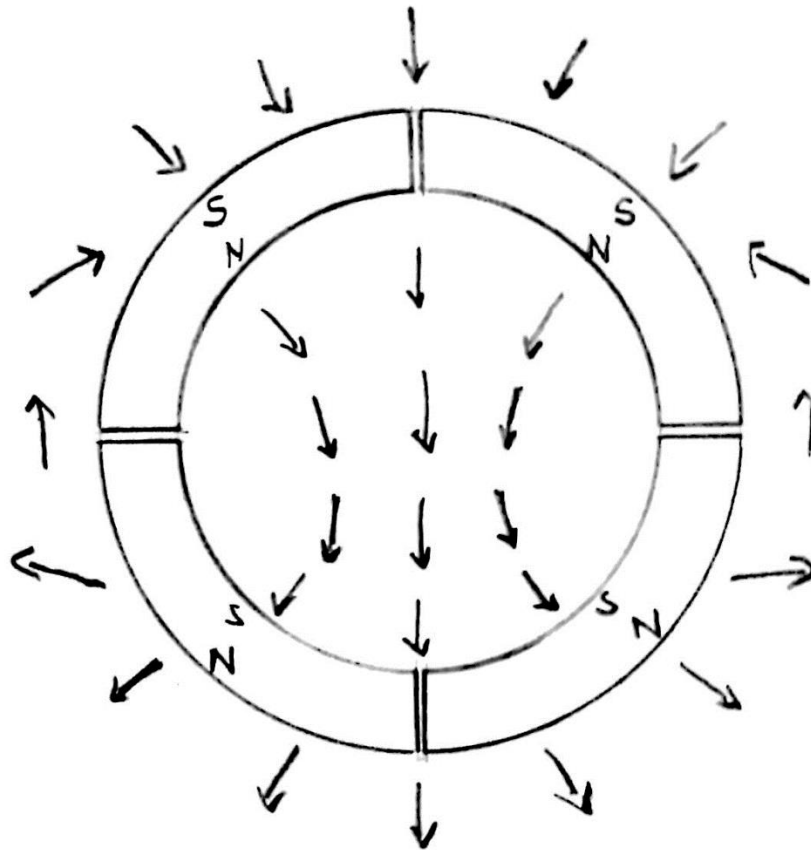
SCALE = 1:3

3.3.5.6 Simulation Results

The magnetic field inside the arrangement was simulated using COMSOL 4.3 and the flux profile and the field strength was studied.
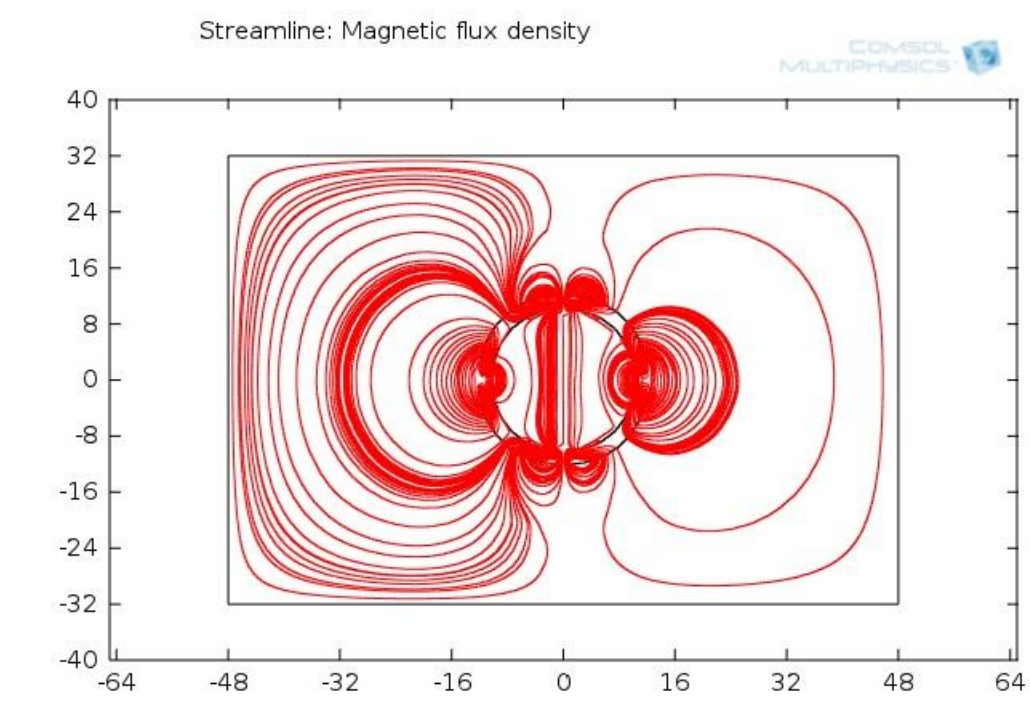
3.3.5.7 Conclusion

The magnet arrangement has a uniform magnetic field and has a strength of ~500 G as found experimentally. The COMSOL simulations are in agreement with the experimentally obtained results.

Chapter 4

Results and Discussions

As a part of this project, the various components of the polarizer designed at INMAS, DRDO was studied and analysed. Simulations were done to understand the overall working mechanism of the components and experiments were carried out to test the components.

4.1 Simulation Results

The results from the simulation of the Helmholtz coil clearly shows that the field in between the coils are uniform and the magnetic field is also large enough (>30G) to bring about efficient optical pumping. The radius for the middle and outer coils in the case of tri-axial Helmholtz coil was calculated. On applying the radius to the model a compact arrangement was obtained. The current through each coil was controlled such that the field produced by each coil is the same. The results shows the uniform field within the coil arrangement. The conductive heat transfer through the Pyrex cylinder was simulated. The results showed the temperature profile in the cross-section. The profile showed the temperature at various widths of the cell. The values of temperature at various points was noted. The turbulent flow through a single turn of the helical condenser coil was simulated. Sufficient cooling takes place in the coil assembly. After passing through the condenser unit the xenon gas would condense and could be accumulated in the phantom. The temperature at inlet is 413.0228 K and at the outlet it is at 278.432 K. With more turns the freezing point of xenon (161.2 K) could be attained. Then various arrangements of magnet for xenon accumulation was modelled. Firstly the already present magnet arrangement consisting of four arc magnets was modelled. The simulations showed uniform magnetic fields of sufficient intensity at the centre. The linear Halbach array and the Halbach cylinder produced even stronger magnetic fields. A simple magnet arrangement consisting of four magnet dipoles was also studied. This was a simple arrangement and could be easily implemented.

4.2 Experimental Results

The magnetic field between the coils of the Helmholtz coil was tested experimentally also. It produces a uniform magnetic field of 34 G. It is sufficient enough to bring about the Zeeman splitting for the optical pumping process. The polarity of the light after leaving the polarizing beam splitter cube and the quarter wave plate was experimented. It was confirmed

that the light leaving the polarizing beam splitter cube was vertically linearly polarized and the light leaving the quarter wave plate inclined at $\pm 45°$ was circularly polarized. The magnetic field strength inside the magnet arrangement for xenon accumulation was tested using a gauss meter and field strength of ~500 G was obtained. The field profile was also tested using a magnetic compass and was found to be uniform. The starting and shutting down procedure of the laser system was studied and discussed.

Chapter 5

Summary and Conclusions

This project was regarding the modelling, simulation and testing of a few components of the polarizer developed at INMAS, DRDO. The polarizer is used to produce large quantities of hyperpolarized xenon used in MRI/ NMR applications. The modelling was done using COMSOL Multiphysics 4.3. It is a comprehensive simulation software environment and has a wide array of applications. It is very user friendly and flexible. It has a number of modules for various applications. Some of the modules used in this project are AC/ DC module, Heat Transfer module, Fluid Flow module and Electromagnetics module. The uni-axial and tri-axial Helmholtz coil was designed using the magnetic field sub module of AC/ DC module. It helped in simulating the magnetic fields due to the current flowing through the multiturn coil taking into account the radius of the coil as well as the distance between the coils. It was possible to plot the flux profile in a particular plane of interest. The 3D model helped in getting a complete understanding of the system. It was possible to turn the model through any degrees and analyse the magnetic field in any plane.

The heat transfer module was used simulate the heat transfer due to conduction in the pumping cell. The 2D axi-symmetric module helped in first creating a 2D model of the cross-section of the cell and then based on the calculation extending it to 3D model. Finally, the 3D system was simulated and the temperature profile was plotted. With the 3D model the system could be viewed from any angles and the temperature at any point could be obtained. With the help of the Heat Transfer module, it was possible to specify the boundary conditions and also the steady state heat transfer equations could be easily implemented on the model. The Fluid Flow module was used to model the turbulent flow through the condenser tubes. It was possible to study the heat transfer and to understand the impact of liquid nitrogen gas on the velocity and the temperature of the fluid flowing through the tube. The non-isothermal flow functionality helped in understanding the fluid and thermal interaction. With various tools in the geometry section the modelling was simplified.

The Electromagnetics module made it possible to simulate various magnet arrangements for its use in the xenon accumulation unit. With the help of this module, the magnet arrangement currently used in the polarizer, a linear Halbach array, Halbach cylinder and also a simple magnet arrangement using four dipoles was simulated. It was possible to

implement magnetization relations and also the directions of magnetizations could be controlled. It was possible to show the strong and uniform magnetic field in the case of linear Halbach array and Halbach cylinder. It was possible to specify the material properties defining each domains. The colour range in the plots could be defined to get more clarity regarding the distribution of the magnetic fields. The testing of various components was also done to understand its performance. Various experiments were conducted to test the magnetic field within the Helmholtz coil, the temperature inside the oven, the polarity of light and the magnetic field strength and uniformity inside the magnet arrangement. The systems were efficient enough to perform polarimetry experiments.

Appendix I

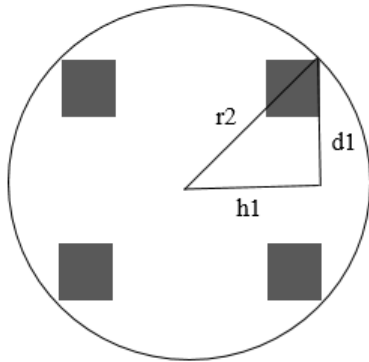## Derivation of the Equation for Radius of Each Coil Pair in Tri-Axial Helmholtz Coil

Fig: center along x axis

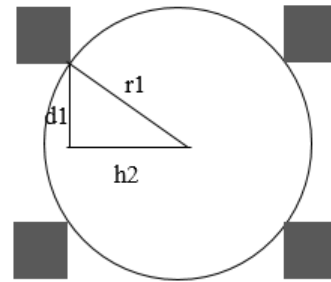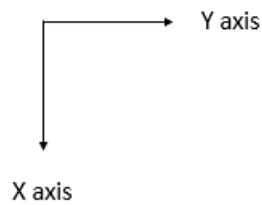Fig: center along y axis

$$d_1{}^2 + h_1{}^2 = r_2{}^2 \qquad -(1)$$

$$d_1{}^2 + h_2{}^2 = r_1{}^2 \qquad -(2)$$

from (2);

$$d_1{}^2 = r_1{}^2 - h_2{}^2 \qquad -(3)$$

substituting (3) in (1),

$$(r_1{}^2 - h_2{}^2) + h_1{}^2 = r_2{}^2 \qquad -(4)$$

Now considering the square geometry of the coils:

$r_1 = R_1 + 2$

$h_2 = \frac{H_2}{2} - 2$

$h_1 = \frac{H_1}{2} + 2$

$r_2 = R_2 - 2$

Now consider the condition of the Helmholtz coil that $R = H$.

So, $R_1 = H_1$ and $R_2 = H_2$

On substituting the values we get,

$$\frac{5}{4}R_2{}^2 - 6R_2 = \frac{5}{4}R_1{}^2 + 6\,R_1 \qquad \text{-(5)}$$

To get the radius of the middle coil, enter the value of the inner coil as R1 and to get the radius of the outer coil, replace R1 by the radius of the second coil.

Literature Cited

1. 1. B. M. Goodson, "Concepts Magn. Reson". 11, 203-223 (1999).

2. T. R. Carver and C. P. Slichter, *Phys. Rev*, 92, 212 (1953).

3. T. R. Carver and C. P. Slichter, *Phys. Rev*, 102, 975 (1956).

4. C. F. Hwang and D. A. Hill, *Phys. Rev. Lett*., 19, 1011 (1967).

5. C. F. Hwang and D. A. Hill, *Phys. Rev. Lett*., 18, 110 (1967).

6. A. W. Overhauser, *Phys. Rev* 92, 411 (1953).

7. P. F. Seldler, H. E. Bryndza, J. E. Frommer, L. S. Stuhl, R. G. Bergman, Synthesis of trinuclear alkylidyne complexes from dinuclear alkyne complexes and metal hydrides. CIDNP for vinyl radical intermediates in the hydrogenolysis of these clusters, *Organometallics* 2, 1701-1705, (1983).

8. C. R. Bowers, D. P. Weitecamp, Parahydrogen and synthesis allow dramatically enhanced nuclear alignment, *J. Am. Chem. Soc.* 109, 5541-5542 (1987)

9. T. C. Eisenschmid, R. U. Kirss, P. P. Deutsch, S. I. Hommeltoft, R. Eisenberg, J. Bargon, R. G. Lawler, A. L.Balch, Parahydrogen induced polarization in hydrogenation reactions, *J. Am. Chem. Soc*. 109, 8089-8091 (1987).

10. L. P. Neukirch and T. J. Gay, Behlen Laboratory of Physics, University of Nebraska, Systematic study of rubidium optical pumping.

11. Christopher Witte, Martin Kunth, Jorg Dopfert, Federica Rosella, Leif Schroder, Hyperpolarized xenon for NMR and MRI applications, *JOVE*, (2012).

12. Duffin, W. J., "Electricity and Magnetism", Fourth edition, McGraw Hill, (1990).

13. John H Lienhard IV and John H Lienhard V, 'A heat transfer textbook', third edition, Phlogyston Press, Cambridge Massachusetts.

14. S. Appelt, T. Unlu, K. Zilles, N. J. Shah, S. Baer-Lang, H. Halling, Experimental studies of rubidium absolute polarization at high temperatures. *Applied Physics Letters*, 75, (1999).

15. R. Beiranvand, Magnetic field uniformity of the practical tri-axial Helmholtz coil systems, *Rev. Sci. Instrum*. 85, (2014).

16. Jai Min Choi, Jang Myun Kim, D. Cho, *Physical review A*, 76, (2007).

17. Paul Siddons, Charles S. Adams, Ifan G. Hughes, *Physical review A*, 81, (2010).

18. S. Li, P. Vachaspati, D. Sheng, N. Dural, M. V. Romalis, Optical rotation in excess of 100 rad generated by Rb vapor in a multipass cell, *Physical review A*, 84, (2011).

19. J. M. Dreiling, E. B. Norrgard, D. Tupa, T. J. Gay, *Physical review A*, 86, (2012).

20. Zhang Qi, Pan Mengchun, Chen Dixiang, Analytic calculation of magnetic field and force in Halbach permenant magnet linear motor, *ICEMI*, (2011).

21. Wenjin Shao, Guodong Wang, Raymond Fuzesy, Emlyn W. Hughes, Blaine A. Chronik, Greig C. Scott, Steven M. Conolly, Albert Macovski, Low readout field magnetic resonance imaging of hyperpolarized xenon and water in a single system, *Applied physics letters*, 90, (2002).

22. B. Driehuys, G. D. Cates, E. Miron, K. Sauer, D. K. Walter, W. Happer, High volume production of laser polarized ^{129}Xe, *Appl. Phys. Lett.* 69, (1996).

23. Panayiotis Nikolaou, Aaron M. Coffey, Laura L. Walkup, Brogan M. Gust, Nicholas Whiting, Hayley Newton, Iga Muradyan, Mikayel Dabaghyan, Kaili Ranta, Gregory D. Moroz, Mathew S. Rosen, Samuel Patz, Michael J. Barlow, Eduard Y. Chekmenev, Boyd M. Goodson, XeNA: An automated open source ^{129}Xe hyperpolarizer for clinical use, *Magnetic resonance imaging*, 32, 541-550,(2014).

24. M. S. Rosen, T. E. Chupp, K. P. Coulter, R. C. Welsh, S. D. Swanson, Polarized ^{129}Xe optical pumping/spin exchange and delivery system for magnetic resonance spectroscopy and imaging studies, *Rev. Sci. Instrum*, Vol 70, No. 2 , (1999).

25. I. C. Ruset, S. Ketel, F. W. Hersman, Optical pumping system design for large production of hyperpolarized ^{129}Xe, *Physical review letters,* 96, (2006).

26. Anthony L. Hook, Bhavin B. Adhyaru, Clifford R. Bowers, High capacity production of >65% spin polarized xenon − 129 for NMR spectroscopy and imaging, *Journal of magnetic resonance,* 159, (2002).

27. M. S. Albert, G. D. Cates, B. Driehuys, W. Happer, B. Saam, C. S. Springer Jr, A. Wishnia, Biological magnetic resonance imaging using laser polarized ^{129}Xe. *Nature* 370, (1994).

28. J. M. Kneller, R. J. Soto, S. E. Surber, J-F. Colomer, A. Fonseca, J. B. Nagy, T. Pietra, *Journal of magnetic resonance*, 147, 261-265 (2000).

29. Mathias Haake, Alexander Pines, Jeffrey A. Reimer, Roberto Seydoux, Surface enhanced NMR using continuous flow laser-polarized xenon, *J Am. Chem. Soc.*,119, (1997).

30. Charles V. Rice, Daniel Raftery, Rubidium xenon spin exchange and relaxation rates measured at high pressure and high magnetic field, *Journal of chemical physics*, 117, (2002).

31. Roberto Seydoux, Alexander Pines, Mathias Haake, Jeffrey A. Reimer, NMR with a continuously circulating flow of laser polarized ^{129}Xe, *J. Phys Chem B,* 103, 4629-4637, (1999).

32. A. V. Kessenikh, V. I. Lushchikov, A. A. Manenkov, and Y. V. Taran, *Sov. Phys. Solid State*, 5, 321 (1963).

33. P.F. Seldler, H.E. Bryndza, J.E. Frommer, L.S. Stuhl, R.G. Bergman, Synthesis of trinuclear alkylidyne complexes from dinuclear alkyne complexes and metal hydrides. CIDNP for vinyl radical intermediates in the hydrogenolysis of these clusters, *Organometallics* 2, 1701–1705, (1983).

34. C.R. Bowers, D.P. Weitekamp, Transformation of symmetrization order to nuclear-spin magnetization by chemical reaction and nuclear magnetic resonance, *Phys. Rev. Lett.* 57 , 2645–2648 , (1986).

35. C.R. Bowers, D.P. Weitekamp, Parahydrogen and synthesis allow dramatically enhanced nuclear alignment, *J. Am. Chem. Soc.* 109, 5541–5542, (1987).

36. Nacher P.J., Leduc M., Optical pumping in 3He with a laser, *Journal de Physique* 46, pp. 2057-2073, 1985.

37. Courtade E., Marion F., Nacher P.J., Tastevin G., Kiersnowski K., Dohnalik T., Magnetic field effects on the 1083 nm atomic line of helium, *The European Physical Journal* D 21, , pp. 25-55, 2002.

38. Fitzgerald R J, Sauer K L and HapperW, Cross-relaxation in laser-polarized liquid xenon *Chem. Phys. Lett.* 284, 87–92, 1998.

39. Tseng C H, Mair R W, Wong G P, Williamson D, Cory D G and Walsworth R L, Magnetic resonance imaging of laser polarized liquid xenon *Phys. Rev.* E 59 1785–8, 1999.

40. Gatzke M, Cates G D, Driehuys B, Fox D, Happer W and Saam B, Extraordinarily slow nuclear spin relaxation in frozen laser-polarized 129Xe *Phys. Rev. Lett.* 70 690–3, 1993.

41. Bowers C R, Long HW, Pietrass T, Gaede H C and Pines A, Cross-polarization from laser-polarized solid xenon to 13CO2 by low-field thermal mixing *Chem. Phys. Lett.* 205 168–70, 1993.

42. Augustine MP,Wong-Foy A, Yarger J L, Tomaselli M, Pines A, TonThat DM and Clarke J, Low field magnetic, resonance images of polarized noble gases obtained with a dc superconducting quantum interference device *Appl. Phys. Lett.* 72 1908–10, 1998.

43. Haake M, Goodson B M, Laws D D, Brunner E, Cyrier M C, Havlin R H and Pines A, NMR of supercritical laser-polarized xenon *Chem. Phys. Lett.* 292 686–90, 1998.

44. Leawoods J C, Saam B T and Conradi M S, Polarization transfer using hyperpolarized, supercritical xenon *Chem. Phys. Lett.* 327 359–63, 2000.

45. Rentzepis P M and Douglass D C Xenon as a solvent *Nature* 293 165–6, 1981.

46. Clever H L (ed) *Krypton, Xenon and Radon–Gas Solubilities* vol 2 (Oxford: Pergamon), 1979.

47. Stillinger F H, Water Revistied *Science* 209 451–7, 1980.

48. Lawrence J H, Loomis W F, Tobias C A and Turpin F H, Preliminary observations on the narcotic effect of xenon with a review of values for solubilities of gases in water and oils *J. Physiol.* 105 197–204, 1946.

49. Cullen S C, Eger E I, Cullen B F and Gregory P,Observations on the anesthetic effect of the combination of xenon and halothane *Anaesthesiology* 31 305–9, 1969.

50. Marx T *et al,* Xenon anaesthesia *J. R. Soc. Med.* 93 513, 2000.

51. Franks N P and Lieb W R, Molecular and cellular mechanisms of general anaesthesia *Nature* 367 607–14, 1994.

52. Meyer K H, Zur Theorie der Alkoholnarkose *Trans. Farad. Soc.* 33 1062, 1899.

53. Overton E, *Studien ̈uber die Narkose, zugleich ein Beitrag zur allgemeinen Pharmakologie* (Jena: Fischer Verlag), 1901.

54. Miller K W, Reo N V, Schoot Uiterkamp A J, Stengle D P, Stengle T R and Williamson K L, Xenon NMR: chemical shifts of a general anesthetic in common solvents, proteins, and membranes *Proc. Natl. Acad. Sci. USA* 78 4946–9, 1981.

55. Rentzepis P M and Douglass D C, Xenon as a solvent *Nature* 293 165–6, 1981.

56. Meersmann T and Haake M, Magnetic field dependent xenon-131 quadrupolar splitting in gas and liquid phase NMR *Phys. Rev. Lett.* 81 1211–4, 1998.

57. Streever R L and Carr H Y, Nuclear magnetic resonance of Xe-129 in natural xenon *Phys. Rev.* 121 20–25, 1961.

58. Hunt E R and Carr H Y, Nuclear magnetic resonance of 129Xe in natural xenon *Phys. Rev.* 130 2302–5, 1963.